AD-A169 318 SIMULATIONS OF SPECIAL INTERIOR BALLISTIC PHENOMENA WITH AND WITHOUT HEAT..(U) ARMY BALLISTIC RESEARCH LAB ABERDEEN PROVING GROUND MD R HEISER ET AL. MAY 86 1/1

UNCLASSIFIED BRL-TR-2732 F/G 19/4 NL

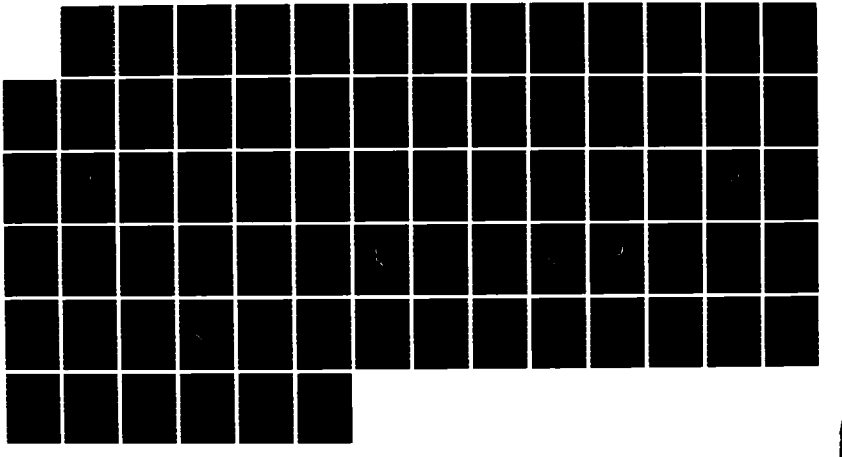

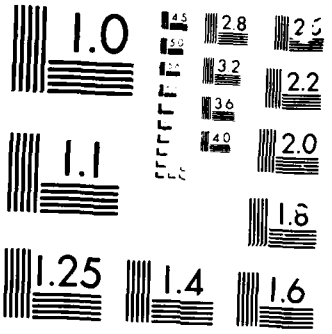

(12)

AD

HD-F 200 780

TECHNICAL REPORT BRL-TR-2732

SIMULATIONS OF SPECIAL INTERIOR BALLISTIC PHENOMENA WITH AND WITHOUT HEAT TRANSFER TO GUN TUBE WALL

Rudi Heiser
James A. Schmitt

May 1986

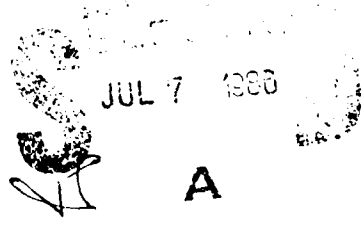

US ARMY BALLISTIC RESEARCH LABORATORY
ABERDEEN PROVING GROUND, MARYLAND

UNCLASSIFIED

SECURITY CLASSIFICATION OF THIS PAGE (When Data Entered)

REPORT DOCUMENTATION PAGE

READ INSTRUCTIONS BEFORE COMPLETING FORM

1. REPORT NUMBER: Technical Report BRL-TR-2732	2. GOVT ACCESSION NO.: ADA 169318
3. RECIPIENT'S CATALOG NUMBER:	
4. TITLE (and Subtitle): Simulations of Special Interior Ballistic Phenomena With and Without Heat Transfer to the Gun Tube Wall	5. TYPE OF REPORT & PERIOD COVERED: Final, Sep 83 - Sep 84
	6. PERFORMING ORG. REPORT NUMBER:
7. AUTHOR(s): Rudi Heiser*, James A. Schmitt	8. CONTRACT OR GRANT NUMBER(s):
9. PERFORMING ORGANIZATION NAME AND ADDRESS: U.S. Army Ballistic Research Laboratory, ATTN: SLCBR-IB, Aberdeen Proving Ground, MD 21005-5066	10. PROGRAM ELEMENT, PROJECT, TASK AREA & WORK UNIT NUMBERS: 1L161102AH43
11. CONTROLLING OFFICE NAME AND ADDRESS: U.S. Army Ballistic Research Laboratory, ATTN: SLCBR-DD-T, Aberdeen Proving Ground, MD 21005-5066	12. REPORT DATE: May 1986
	13. NUMBER OF PAGES: 73
14. MONITORING AGENCY NAME & ADDRESS (if different from Controlling Office):	15. SECURITY CLASS (of this report): Unclassified
	15a. DECLASSIFICATION/DOWNGRADING SCHEDULE:

16. DISTRIBUTION STATEMENT (of this Report)

Approved for Public Release; Distribution Unlimited.

17. DISTRIBUTION STATEMENT (of the abstract entered in Block 20, if different from Report)

18. SUPPLEMENTARY NOTES

*Dr. Rudi Heiser spent a year at the Ballistic Research Laboratory as a visiting scientist from Ernst-Mach Institut at Weil am Rhein in the Federal Republic of Germany

19. KEY WORDS (Continue on reverse side if necessary and identify by block number)

Interior Ballistics	Computer Code	Multidimensional Multiphase Flow
Heat Transfer	Turbulence	ADI Finite Difference Method
Numerical Simulations	One-Phase Flow Results	

20. ABSTRACT (Continue on reverse side if necessary and identify by block number)

The computer code DELTA uses a linearized Alternating Direction Implicit (ADI) scheme to provide a numerical approximation of the solution of the averaged two-phase (gas-solid) two-dimensional (axisymmetric) equations governing viscous interior ballistic flows within conventional guns. To further the understanding of phenomena affecting gun tube life as well as gun performance, a heat transfer model, which simulates the interactions of fluid dynamics and thermal profile in the gun tube wall, has been

DD FORM 1 JAN 73 1473 EDITION OF 1 NOV 65 IS OBSOLETE

UNCLASSIFIED

SECURITY CLASSIFICATION OF THIS PAGE (When Data Entered)

incorporated in the DELTA code. The same linearized ADI method was utilized to obtain the numerical solution of the two-dimensional nonlinear heat conduction equations in the gun tube. Our model of the heat transfer process couples completely and simultaneously all three controlling events without any approximations to the governing equations; that is, the axisymmetric viscous flow within the entire gun tube which naturally gives a precise definition of the gas thermal boundary layer, the time-dependent balance of the heat fluxes at the inner wall surface, and the two-dimensional temperature calculation within the gun tube wall. The nonlinear heat flux boundary conditions at the inner and outer tube surfaces are linearized to be compatible with the solution scheme.

Results computed with DELTA are presented for two different types of idealized one-phase interior ballistics flows. The first is a pure expansion flow, and the other includes mass and heat sources. For each of the flows we present the effects of gas turbulence and the effects of heat conduction to the wall. Our results indicate that both effects are significant.

TABLE OF CONTENTS

LIST OF ILLUSTRATIONS

LIST OF ILLUSTRATIONS (CONT'D)

LIST OF ILLUSTRATIONS (CONT'D)

LIST OF ILLUSTRATIONS (CONT'D)

I. INTRODUCTION

Interior ballistics flows of conventional charges in gun tubes possess complex flow patterns. Their complexity is due to both the heterogeneous structure of the charge and the rapidly changing flow conditions within a few milliseconds. The fast rise in pressure and temperature caused by the burning of the propellant initiates a turbulent, multidimensional, multiphase flow which is coupled with the accelerating projectile motion. A complete mathematical model that describes all the physical phenomena occurring in an interior ballistics cycle is not presently available. However, several models that simulate some of the phenomena exist or are being developed.[1]

On the other hand, it is not possible for technical reasons to make detailed experimental measurements of the complete interior ballistic cycle. Some standard techniques as well as some new special techniques under development determine only specific quantities in real weapons or in simulators under simplified flow conditions. Commonly measured quantities are the gas pressure and projectile motion. Other quantities such as the temperature distribution in the gas and in the gun tube wall, the velocity distribution of the gas and solid particles inside or outside of boundary layers, the particle distribution, the turbulence pattern, etc., cannot be accurately determined by experiment. Thus, a need exists for modelling of the interior ballistic cycle so that the dynamic development of these quantities can be studied, and their impact on ballistic problems can be evaluated.

A new computational capability for the investigation of interior ballistics flows is the DELTA code, which is under development at the Ballistic Research Laboratory. The purpose of this code is to address particular ballistics problems related to the boundary layer development, the heat transfer to the tube wall, the turbulence, and the time-dependent distribution of additive particles. In the following, we shall give a short description of the DELTA code and present computational results of an investigation of heat conduction and turbulence effects.

II. REVIEW OF THE MODELS IN DELTA

The flow which is modeled by DELTA is a multidimensional, two-phase flow inside a gun tube. Presently, the flow is assumed to be axisymmetric. At the rear end, the so-called breech, the tube is closed by a stationary flat plate while the front boundary is a moving flat-based projectile. The flow is assumed to be viscous and heat conducting, and it can be either laminar or

---

[1] "Fluid Dynamics Aspects of Internal Ballistics," AGARD Advisory Report No. 172, 1982.

turbulent. The wall may be either adiabatic or it may allow heat transfer from the gas. Heat transfer is restricted to the tube wall (excluding the breech). The core flow is fully coupled to the moving projectile, to the boundary layer development and, if desired, to the heat conduction in the tube wall. By fully coupled we mean that each of these phenomena can affect all others. For example, the boundary layer development can alter the details of the core flow. This would not be the case, for example, in a boundary layer type model.

The mathematical model in DELTA (the balance equations for the gas-phase and one solid phase), is based on an unsteady volume-averaged formulation. The gas phase is described by averaged equations corresponding to the full Navier-Stokes equations for a compressible fluid. The model is closed by averaged coefficients of viscosity and heat conduction, an averaged viscous stress tensor, an averaged dissipation function and an averaged heat conduction function. Since interior ballistics flows usually produce high gas pressures, the Noble-Abel equation of state is used so that some real gas effects can be included. The gas turbulence is represented by algebraic mixing length models. The solid phase is described by the averaged equations for arrays of incompressible particles which can undergo deformations. The derivation of the equations is given in Ref. 2. The equations of the solution algorithms are listed in Ref. 3.

The system of partial differential equations for the axisymmetric two-phase flow region is solved by a linearized Alternating Direction Implicit (ADI) scheme. This scheme transforms the differential equations into a system of linear algebraic equations. The corresponding matrix has a block tridiagonal structure, allowing an efficient determination of the solution at each new time-step. Details about the derivation of the scheme are presented in Ref. 3.

III. HEAT TRANSFER TO AND TEMPERATURE DISTRIBUTION IN THE TUBE WALL

The heating of the gun tube wall caused by convection, heat conduction, and radiation of the hot propellant gas enhances the gun tube wear and erosion, and therefore, affects the lifetime of gun tubes. An experimental determination of the inner wall surface temperature is quite difficult. Commonly used thermocouples are of limited use in interior ballistic

---

[2]Gelmins, A.K.R., Schmitt, J.A., "Three-Dimensional Modeling of Gas-Combusting Solid Two-Phase Flows," Multi-Phase Flow and Heat Transfer III, Part B: Applications, T. N. Veziroglu and A.E. Bergles, editors, pp. 681-698, Elsevier Science Publishers, Amsterdam, 1984.

[3]Schmitt, J.A., "A Numerical Algorithm for the Multidimensional, Multiphase, Viscous Equations of Interior Ballistics," Transactions of the Second Army Conference on Applied Mathematics and Computing, ARO-Report 85-1, pp. 649-691, 1985.

applications because such applications require accurate measurements in very short time intervals, a close contact to the flow, and special thermal properties of the gauges.

There are several mathematical models of the heat transfer to the gun tube wall. They can be divided in four categories according to their complexity. The first type uses a very simplistic boundary layer calculation and a heat transfer correlation, e.g., Colburn's analogy, to obtain the heat transfer.[4-6] Heat losses in the core flow are considered. The empirical heat transfer correlations are derived for fully developed, steady, one-phase pipe flow. The main feature of this type of model is the emphasis on the calculation of the core flow. In models of the second category the emphasis is on a description of the boundary layer by using more general boundary layer equations.[7,8] The heat transfer to the tube wall again is described by correlations. The boundary layer edge is not coupled with the computation of the core flow. Instead, one assumes for the latter values which represent approximately the core flow. The third category makes use of general boundary layer equations and of a balance of heat fluxes from the hot gas to the gun tube wall at the inner wall surface.[9] The conditions at the boundary layer edge are comparable to those in the second category. Neither of these approaches includes all the feedback mechanisms from the tube to the core flow, and therefore, to the projectile motion. The fourth category of models uses a fully coupled approach whereby the phenomena in the core flow are directly linked to the projectile motion, the boundary layer development, the heat transfer to and the heat conduction in the tube wall, and vice versa. This is achieved by using a single system of equations everywhere in the gas region and a coupled system of heat conduction equations in the tube wall. The solution of these sets automatically provides the boundary layer solution in the boundary layer region, the core flow solution in the core flow, and all the necessary coupling that naturally occurs in the flow. Although this type

---

[4] Shelton, S., Bergles, A., Saha, P., "Study of Heat Transfer and Erosion in Gun Barrels," Air Force Armament Laboratory, Eglin Air Force Base, Florida, AFATL-TR-73-69, 1973.

[5] Gough, P., "Modeling of Rigidized Gun Propelling Charges," Ballistic Research Laboratory, Aberdeen Proving Ground, Maryland ARBRL-CR-00518, 1983.

[6] Nelson, C.W., Ward, J.F., "Calculation of Heat Transfer to the Gun Barrel Wall," J. Ballistics 6 (3), pp. 1518-1524, 1982.

[7] Barlett, E.P., Anderson, L.W., Kendall, R.M., "Time-Dependent Boundary Layers with Application to Gun Barrel Heat Transfer," Proceedings 1972 Heat Transfer Fluid Mech. Institute, Stanford University, CA, 1972.

[8] Buckingham, A.C., "Modeling Propellant Combustion Interacting with an Eroding Solid Surface," Lawrence Livermore Laboratory, UCRL-83727, 1980.

[9] Adams, M.J., Grier, N., "Unsteady Internal Boundary Layer Analysis Applied to Gun Barrel Wall Heat Transfer," Int. J. Heat Mass Transfer, Vol. 24, No. 12, pp. 1925-1935, 1981.

of solution is most complex, it provides a flow description with the fewest assumptions and approximations. In light of the scarcity of experimental measurements with which to compare the calculations, we feel such an approach to be best. The DELTA code is an example of a fourth category model.

The heat transfer model in DELTA consists of the equations governing the heat conduction in the tube wall, and the boundary conditions which couple the temperature in the wall to the flow inside and outside the tube. The heat conduction in the tube wall is described by the two-dimensional, nonlinear axisymmetric equation for the wall temperature $T_w(t,r,z)$:

$$\rho_w(T_w)\ c_w(T_w)\ \frac{\partial T_w}{\partial t} = \frac{\partial}{\partial z}\left[\lambda_w(T_w)\ \frac{\partial T_w}{\partial z}\right]$$

$$+ \frac{1}{r}\ \frac{\partial}{\partial r}\left[r\ \lambda_w(T_w)\ \frac{\partial T_w}{\partial r}\right] .$$

The variables t, z and r denote the time, axial coordinate in the wall and radial coordinate in the wall, respectively. The specific heat c_w and the thermal conductivity λ_w of gun tube steel strongly depend on the temperature.[10] By comparision, the density of the steel ρ_w varies only a little with temperature.

The most important boundary condition is at the inner tube wall surface where the coupling of the flow region and the wall occurs. It consists of the balance of heat fluxes with a radiation effect

$$-\lambda_g\ \frac{\partial T_g}{\partial r_g} + \varepsilon\ \sigma\ (T_{g_o}^4 - T_g^4) = -\lambda_w\ \frac{\partial T_w}{\partial r}$$

and of the temperature equilibrium equation

$$T_g = T_w .$$

The variables λ_g, ε, σ, T_g and T_{g_o} denote the thermal conductivity of the gas, the emissivity of the wall surface, the Stefan-Boltzmann constant, the gas temperature, and the maximum gas temperature in a given cross-section (z = constant), respectively. We emphasize that in DELTA both conditions are used only at the inner tube wall surface, excluding the breech. The left hand side of the first condition represents the heat flux on the gas side towards the wall, whereby the first term represents heat conduction, and the second term represents heat radiation. The right hand side gives the heat flux into the tube wall. For the boundary conditions at the outer tube wall surface we

---

[10] Aerospace Structural Metal Handbook, "Ferrous Alloys," 1973.

chose the simple engineering condition

$$- \lambda_w \frac{\partial T_w}{\partial r} = h \, (T_w - T_{amb}) \, ,$$

where h is a heat transfer coefficient and T_{amb} is an outer ambient temperature. A more sophisticated condition is not needed (at least for a single shot weapon) because the heat usually does not reach the outer surface during a ballistic cycle. Two additional boundary conditions are needed in axial direction. At the projectile base, we set

$$T_w = T_{amb},$$

across the wall thickness, that is, we assume that the projectile moves into an area which is at ambient temperature. At the breech and at the projectile base, an adiabatic condition

$$\frac{\partial T_g}{\partial z} = 0$$

was assumed to be adequate.

The equations governing the temperature distribution in the tube wall are solved using the same linearized ADI method as for the equations in the gas flow region; that is, the equations are linearized in time, and are split along coordinate directions. At each new time level, we first update the temperature distribution in the wall, and then update the dependent variables in the flow region. This is performed by the following sequence of sweeps along coordinate directions: an axial sweep followed by a radial sweep in the wall, a radial sweep followed by an axial sweep in the gas region, and finally an adjustment of the dependent variables along the inner wall surface to the flux boundary condition. We omit a discussion of the details of the numerical procedure because they are discussed in Ref. 3. In the DELTA code, the thermodynamic dependent variables in the gas region are the specific gas entropy (s) and the logarithm of the gas pressure (q). Therefore, the heat flux boundary condition must be reformulated in terms of s and q at the new unknown time level for the radial sweep in the gas region. To this end, we transform the heat flux term on the right hand side of the condition via the chain rule as follows:

$$\lambda \frac{\partial T}{\partial r} = \lambda(T(s,q)) \frac{\partial T(s,q)}{\partial r} = \lambda(T(s,q)) \left[T_s \frac{\partial s}{\partial r} + T_q \frac{\partial q}{\partial r} \right] ,$$

where T is the gas temperature, and T_s, T_q denote the partial deriviatives of f with respect to s and q, respectively. (For simplicity, we dropped the index g.) The linearization in time gives a relation between the unknown new time level (n) and the known current time level (c)

$$\lambda^n \left(\frac{\partial T^n}{\partial r}\right) = \lambda^c \left(\frac{\partial T^c}{\partial r}\right) + \frac{d}{dt}\left[\lambda \frac{\partial T}{\partial r}\right]^c \Delta t + O(\Delta t^2)$$

with

$$\frac{d}{dt}\left[\lambda \frac{\partial T}{\partial r}\right]^c \Delta t = \left(\frac{d\lambda}{dT}\right)^c \left[T_s^c \frac{ds}{dt} + T_q^c \frac{dq}{dt}\right] \left(\frac{\partial T}{\partial r}\right)^c \Delta t$$
$$+ \lambda^c \left[\left(T_{qq} \frac{\partial q}{\partial r} + T_{sq} \frac{\partial s}{\partial r}\right)^c \frac{dq}{dt} + \left(T_{ss} \frac{\partial s}{\partial r} + T_{qs} \frac{\partial q}{\partial r}\right)^c \frac{ds}{dt}\right] \Delta t .$$

The time-deriviatives we approximate by

$$\frac{ds}{dt} \Delta t \approx s^n - s^c,$$

and

$$\frac{dq}{dt} \Delta t \approx q^n - q^c.$$

With this approximation, the boundary condition provides a linear equation for s^n and q^n. The equation is compatible with the set of finite differenced and linearized flow equations.

IV. TURBULENCE MODEL

In order to estimate the influence of turbulence on the flow pattern, we used two turbulence models. Both were equilibrium algebraic eddy viscosity models based on Prandtl's mixing length hypothesis. In these models, a turbulent eddy viscosity μ_t and a turbulent thermal conductivity λ_t are added to the molecular viscosity μ and thermal conductivity λ, respectively, yielding the effective values

$$\mu_{eff} = \mu + \mu_t,$$

and

$$\lambda_{eff} = \lambda + \lambda_t,$$

which then are used in the laminar flow equations. The two models differ in the underlying assumption that the boundary layer consists either of one region or is composed of two regions.

The one-layer model expresses the turbulent eddy viscosity by

$$\mu_t = \rho \, \ell^2 \left| \frac{\partial w}{\partial r} + \frac{\partial u}{\partial z} \right|,$$

where ρ is the local density, ℓ is Prandtl's mixing length, w and u are the velocity in axial and radial direction, respectively.[11] In the DELTA test calculations the velocity gradients were obtained from the solution of the governing differential equations. The mixing length was obtained from a correlation. For a steady incompressible flow in a tube Nikuradse[11] experimentally determined that

$$\ell = R \left[0.14 - 0.08 \left(1 - \frac{y}{R}\right)^2 - 0.06 \left(1 - \frac{y}{R}\right)^4 \right].$$

where R is the tube radius and y is the distance from the tube wall. Using this correlation one assumes that it models the turbulence also in an unsteady and compressible flow. We test this assumption by comparing the computed results with those obtained using another turbulence model, a so-called two-layer model.

The two-layer model separates the boundary layer in an inner and outer region with different formulations for each region.[12] [13] The expression for the eddy viscosity in the inner region is

$$\mu_{t_{in}} = \rho \, \ell^2 \left| \frac{\partial w}{\partial r} + \frac{\partial u}{\partial z} \right|,$$

which is the same as the one-layer formulation. The difference is in the definition of the mixing length ℓ, which now is calculated by

$$\ell = \hat{k} \, y \, D,$$

where $\hat{k} = 0.4$ is the von Kármán constant, y is the distance from the wall and D is the van Driest damping factor. The latter is given by

$$D = 1 - e^{-\frac{y^+}{A^+}},$$

---

[11] Schlichting, H., "Boundary Layer Theory," McGraw-Hill, 1968.

[12] Rubesin, M.W., "Numerical Turbulence Modeling," AGARD-LS-86.

[13] Kussoy, M.I., Viegas, J.R., Horstman, C.C., "Investigation of a Three-Dimensional Shock Wave Separated Turbulent Boundary Layer," AIAA J., Vol. 18 (1980), No. 12, pp. 1477.

where

$$y^+ = \frac{y}{\mu_w}\sqrt{\rho_w \tau_w}$$

and $A^+ = 26$ is the van Driest constant. The subscript w indicates that the subscripted quantities are to be evaluated at the wall surface (y=0). The wall shear stress τ_w is expressed by

$$\tau_w = \mu_w \left(\frac{\partial w}{\partial y}\right)\Big|_{y=0}.$$

In the outer layer we use for the eddy viscosity the correlation

$$\mu_{t_{out}} = \frac{0.0168\ \rho\ w_e\ \delta^*}{[1 + 5.5\ (y/\delta)^6]},$$

where w_e denotes the axial edge velocity, δ^* the kinematic boundary layer displacement thickness and δ the boundary layer thickness. In our case w_e is the maximum axial velocity in the cross-section z=constant, that is, the velocity on the axis of symmetry. Hence the outer layer encompasses in this model the core flow. The complete two-layer eddy viscosity is given by

$$\mu_t = \begin{cases} \mu_{t_{in}} & \text{if } y < y_c \\ \mu_{t_{out}} & \text{if } y > y_c \end{cases},$$

where y_c is the first point at which $\mu_{t_{in}}$ exceeds $\mu_{t_{out}}$.

The turbulent thermal conductivity is calculated in both cases by

$$\lambda_t = \frac{\mu_t \cdot c_p}{Pr_t},$$

where $Pr_t = 0.9$ is the turbulent Prandtl number and c_p is the specific heat at constant pressure.

V. RESULTS

Computational results are presented for two different types of interior ballistics flows. The first type simulates a pure gas expansion flow behind a projectile moving in a constant cross-section tube. The tube is closed at one end by a stationary surface called the breech, and at the other end by the movable flat based projectile. The initial states of the gas are uniform and quiescent. Geometrical data, initial conditions as well as the thermodynamic properties of the gas are listed in Table I. We designate this idealization as the Lagrange gun.

TABLE I. LAGRANGE GUN PARAMETERS

Bore Diameter	20 mm
Tube Length	2.0 m
Chamber Length	0.175 m
Projectile Mass	120 g
Ratio of Specific Heats	1.271
Covolume	1.08×10^{-3} m^3/kg
Molar Mass	23.8 g/mole
Initial Gas Pressure	300 MPa
Initial Gas Temperature	3000 K
Initial Velocities	0 m/s

The flow in the Lagrange gun is very well suited for the study of several important features such as the performance of the numerical procedure, the boundary layer development, the laminar and turbulent axisymmetric flow patterns, and the heat transfer to the tube wall.

Since an expansion flow is quite removed from the phenomena occurring during a ballistic cycle, a second type of flow is simulated which has time-dependent pressure and temperature profiles similar to a real weapon. It is obtained by adding proper heat and mass to the one-phase flow via source terms. An empirical burning law for pressure-dependent sources is used. The sources move with the flow. We designate this idealization as the "real gun". The essential parameters for the real gun differ from Table I only with respect to the initial conditions. The initial gas pressure is assumed to be ambient pressure (0.1 MPa) and the initial gas temperature to be ambient temperature (293 K). In all cases involving the real gun simulation, the projectile is released from its initial position when the pressure at the projectile base reaches 30 MPa.

Because the DELTA code is based on an implicit finite difference scheme, no stability condition restricts the size of the time step. The presented results are all calculated using a constant time-step of 1.0 μs . The computational mesh consists of 49 uniformly or nonuniformly spaced mesh points

in the axial direction and 19 nonuniformly spaced mesh points in the radial direction. To obtain a finer spatial resolution in the boundary region, the mesh points are concentrated near the wall. An example of a 19x49 computational mesh, which is used in most of the computations, is shown in Figure 1. The smallest grid size in radial direction at the bore surface is 7.7 μm . The mesh for computing the heat conduction in the tube wall is generated in the same way with the same mesh distribution in axial direction as on the gas side, and a corresponding mesh concentration near the inner bore surface. Both the size of time-step and the number of grid points seem to be reasonable compromises between accuracy and computing time.

Some of the computed results for the Lagrange and real gun, respectively, with laminar flows and adiabatic boundaries are compared in Figures 2-5. The figures show the histories of the gas pressures and temperatures at the center of the breech and projectile, and the velocities and displacements of the projectile. The main differences are in the temporal distributions of all quantities shown, and between the final values of the muzzle velocities. In the real gun simulations, the pressure at the projectile base reaches 30 MPa at about 2.3 ms, at which time the projectile begins to accelerate down the tube.

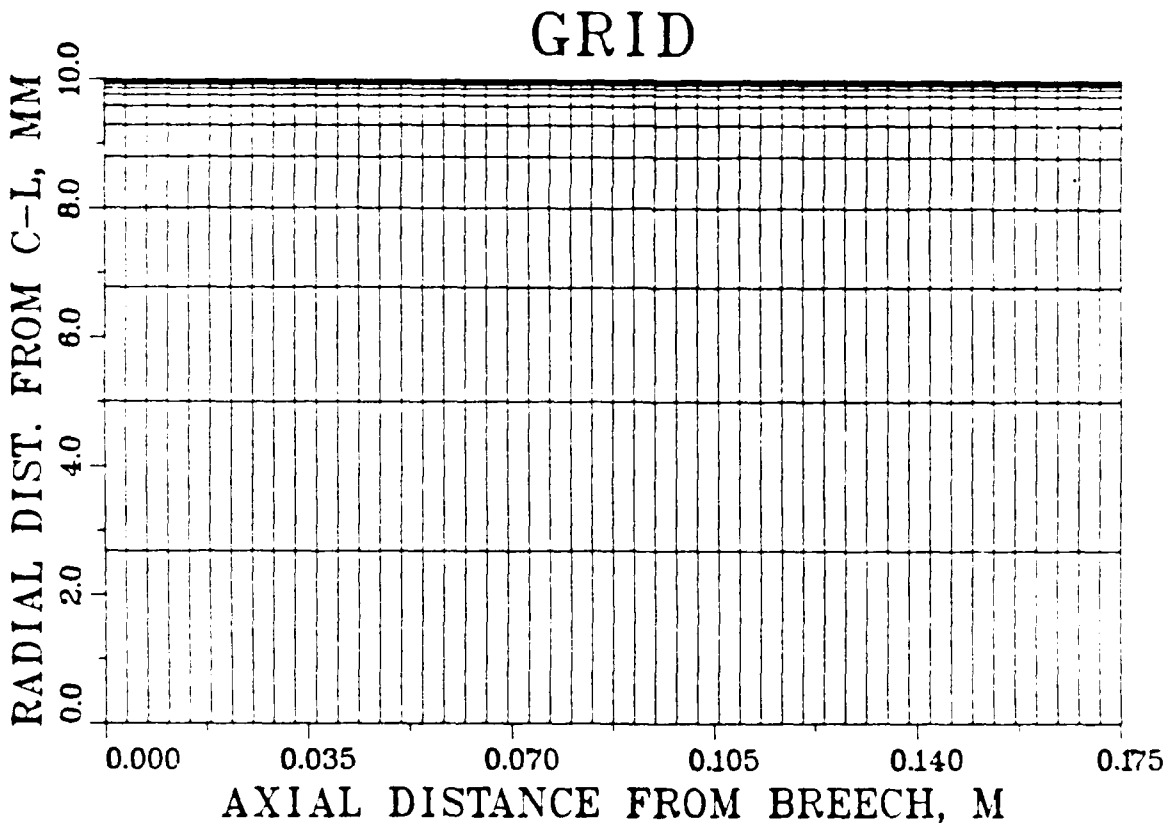

Figure 1. Standard Computational Mesh 19 x 49. Minimum Radial Grid Size is 7.7 μm.

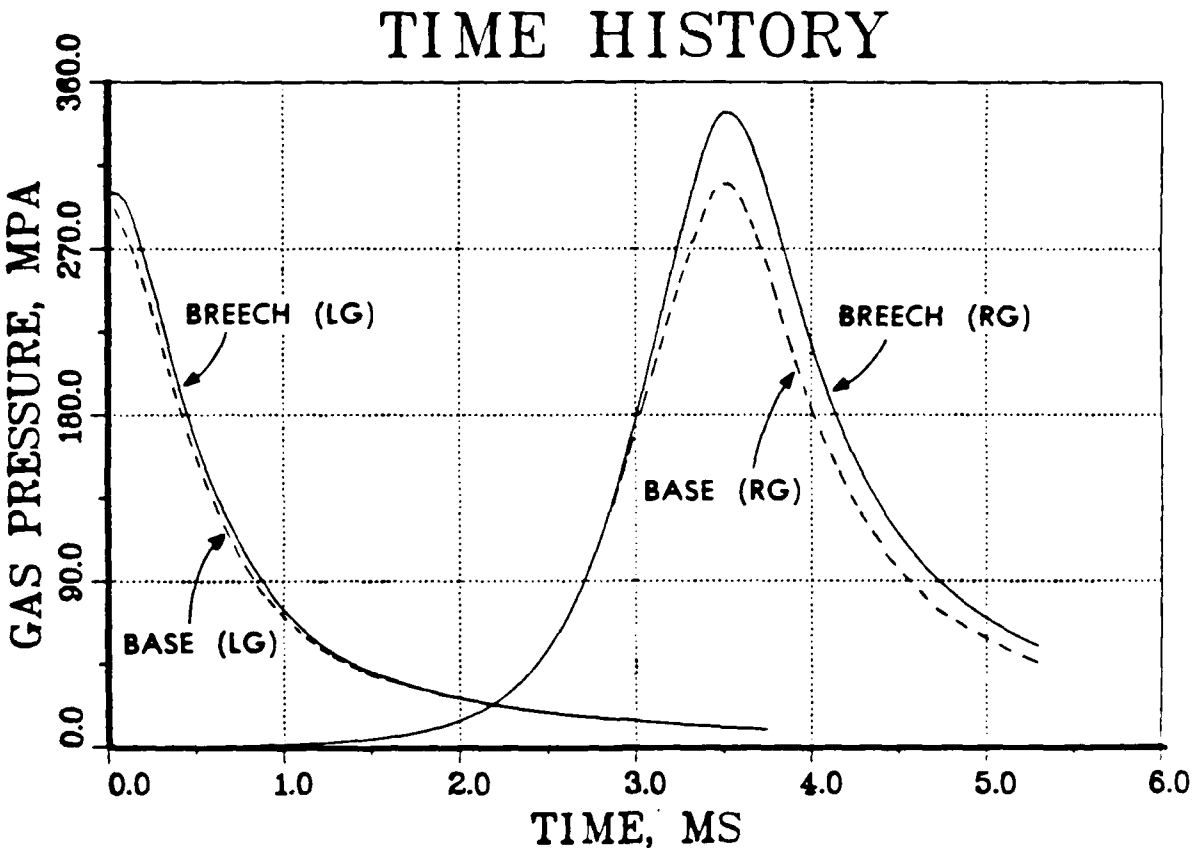

Figure 2. Pressure Histories at the Center of the Breech and the Projectile Base for the Laminar Flow with the Adiabatic Walls in the Lagrange Gun (LG) and the Real Gun (RG) Simulations.

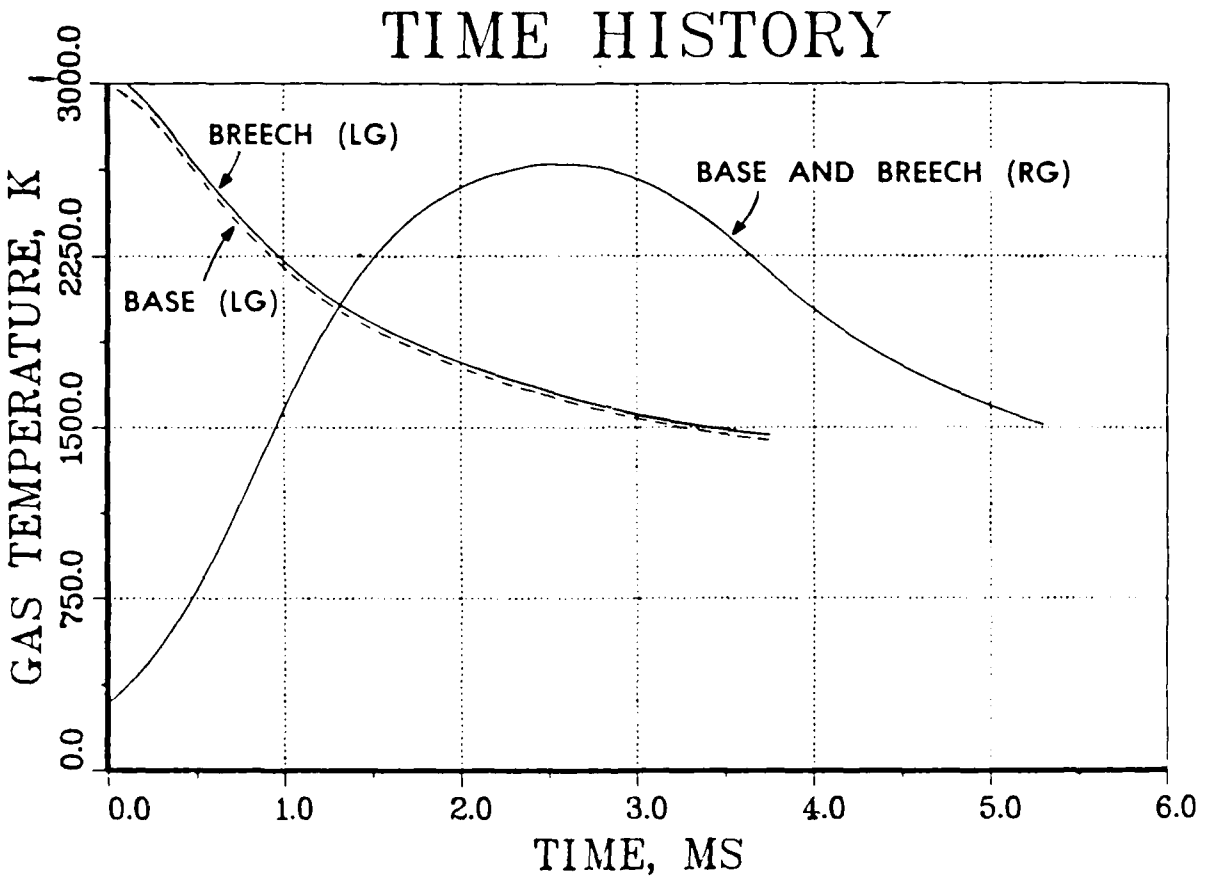

Figure 3. Temperature Histories at the Center of the Breech and the Projectile Base for Laminar Flow with Adiabatic Walls for the Lagrange Gun (LG) and Real Gun (RG) Simulations.

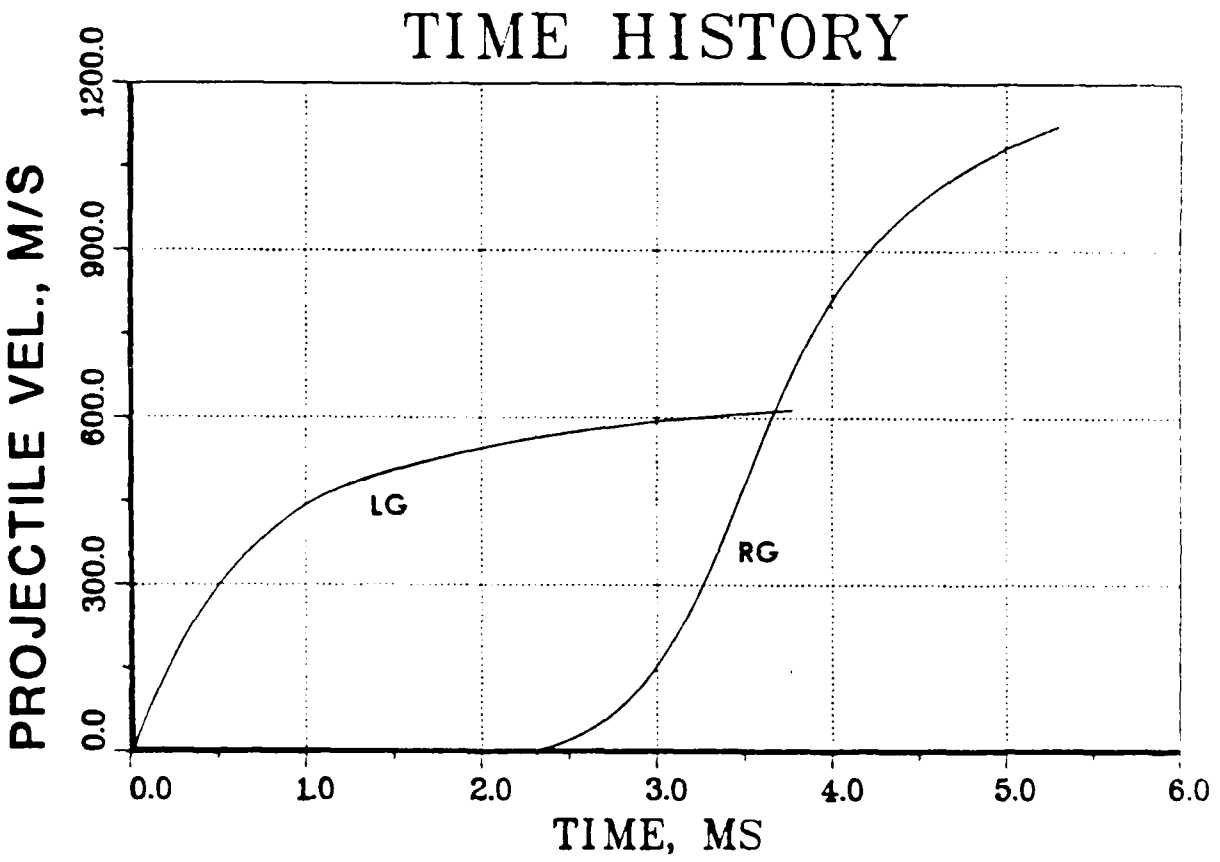

Figure 4. Projectile Velocity Histories for Laminar Flow with Adiabatic Walls in the Lagrange Gun (LG) and Real Gun (RG) Simulations.

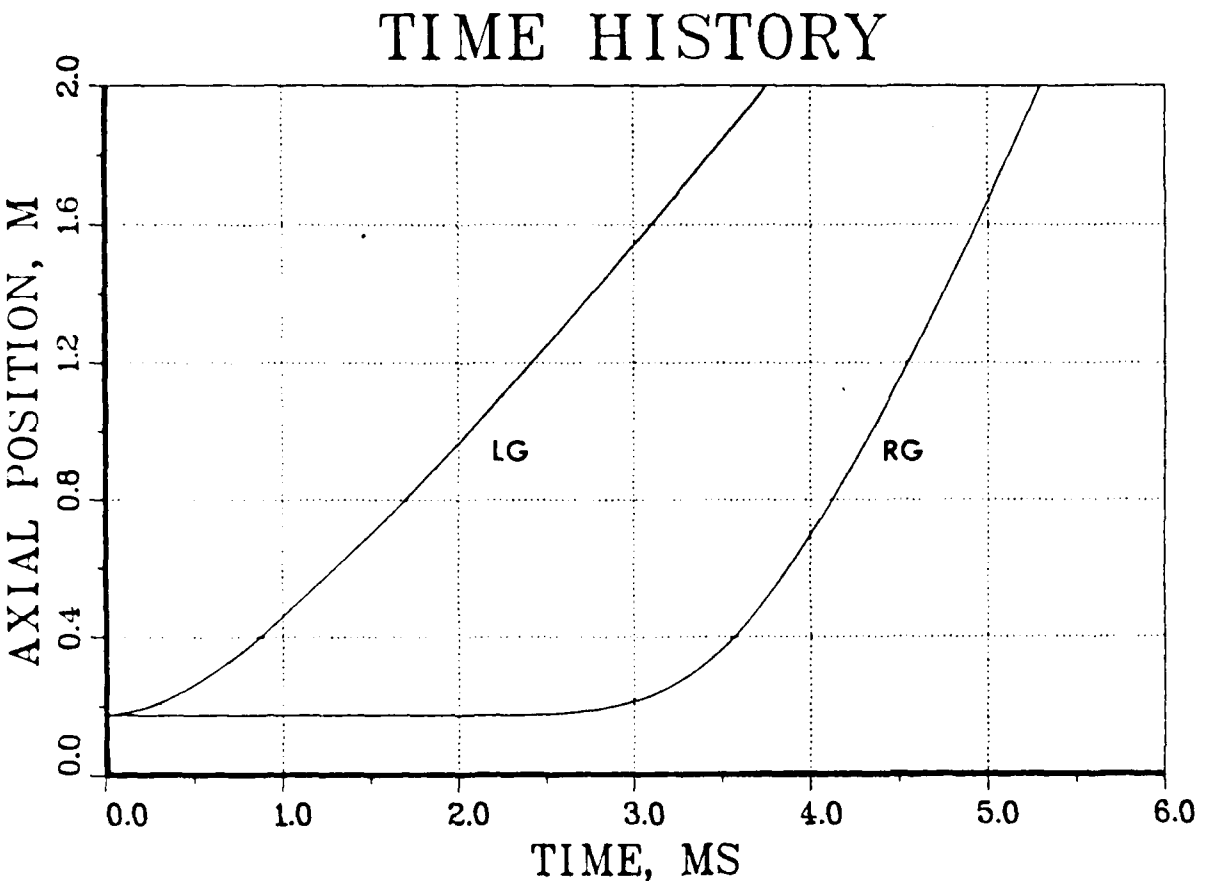

Figure 5. Projectile Displacement from the Breech for Laminar Flow with Adiabatic Walls in the Lagrange Gun (LG) and Real Gun (RG) Simulations.

Detailed qualitative results for a Lagrange gun with a laminar flow and adiabatic walls are presented in Figures 6-10. Notice that the three-dimensional surfaces are shown from different directions in order to make their display clearer. The spatial distribution of the axial velocity is shown in Figures 6 and 7 at 3.75 ms. At this time, the projectile exits the gun tube with a muzzle velocity of 623 m/s. Figure 6 shows the axial velocity field when a uniformly axially spaced mesh as in Figure 1 is used. Figure 7 shows the same quantity but computed using a nonuniformly spaced axial mesh. The radial distribution of the mesh points are the same in both figures. For a given axial position the axial velocity is constant across much of the radius of the tube (the core flow region), and decreases to zero only very close to the wall (the boundary layer region). The boundary layer is the result of the no-slip condition (w=0) at the wall. The thickness of the boundary layer is approximately 0.2 to 0.3 mm. In the axial direction, the velocity is distributed linearly in the core region between the zero value at the breech and the muzzle velocity. The three-dimensional temperature and pressure distributions are given in Figures 8 and 9. Due to the adiabatic boundary condition at the wall surface the heat generated by the viscous forces near the tube wall cannot transfer to the tube wall, and the gas temperature rises towards the wall surface. Here again the boundary layer is only 0.2 to 0.3 mm thick. The pressure, however, stays constant in radial direction over the entire cross-section. The assumption in boundary layer theory that the radial pressure gradient is zero would be valid in this example. Figure 10 shows the 3-D graph of the radial gas velocity. In approximately the first 70% of the distance to the projectile, the radial velocity is negative, i.e., the flow is directed towards the center line (C-L). Thereafter, it is positive and increases remarkably towards the projectile base. Only very close to the projectile does the value of the radial velocity drop rapidly from its maximum value to zero. Of course, the radial velocity is small in comparison to the axial velocity since it is induced only by molecular viscosity and heat conductivity. The results in Figures 2-10 agree very well with both a one-dimensional solution of the core flow using the method of characteristics, and the two-dimensional numerical calculations of Heiser and Hensel.[14,15]

---

[14] Heiser, W., Hensel, D., "AMI: Ein Axialsymmetrisches Modell der Innenballistik, Teil 1: Laminare Einphasenströmung ohne Wärmeübergang (AMI: An Axisymmetric Model of Interior Ballistics, Part 1: Laminar One-Phase Flow without Heat Transfer)," Fraunhofer-Institut für Kurzzeitdynamik, Ernst-Mach-Institut, Abteilung für Ballistik, Weil am Rhein, FRG, Report No. 4/80, 1980.

[15] Heiser, R., Hensel, D., "Berechnung der Gasströmung in einem Waffenrohr mit Hilfe des zweidimensionalen AMI-Modells (Calculation of the Gas Flow Inside a Gun Tube Using the Two-Dimensional AMI Model)." Fraunhofer-Institut für Kurzzeitdynamik, Ernst-Mach-Institut, Abteiling für Ballistik, Weil am Rhein, FRG, Report No. E 1/81, 1981.

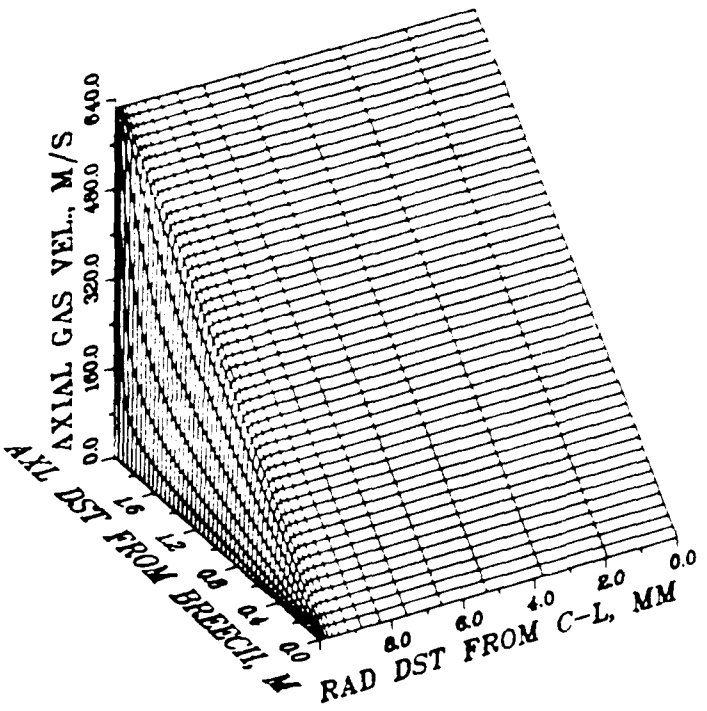

Figure 6. Lagrange Gun, Laminar Flow, Adiabatic Walls: Spatial Distribution of the Axial Gas Velocity at the Time of Muzzle Clearance. Mesh is Uniformly Spaced in Axial Direction and Nonuniformly Spaced in Radial Direction.

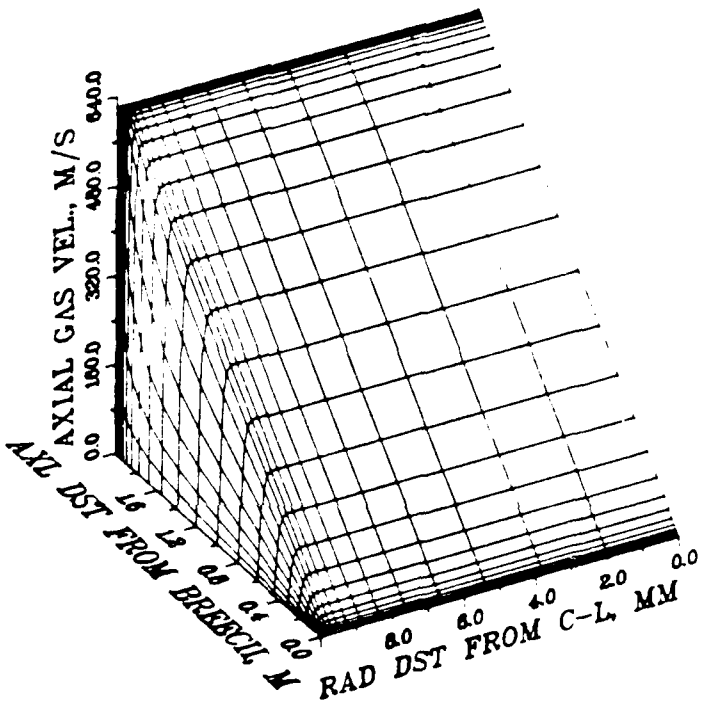

Figure 7. Lagrange Gun, Laminar Flow, Adiabatic Walls: Spatial Distribution of the Axial Gas Velocity at the Time of Muzzle Clearance. Mesh is Nonuniformly Spaced in Both Direction.

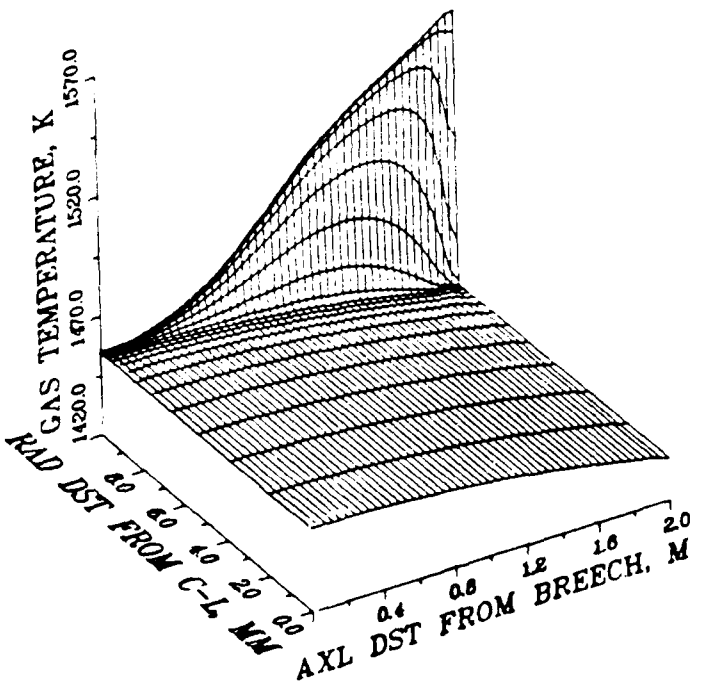

Figure 8. Lagrange Gun, Laminar Flow, Adiabatic Walls: Spatial Distribution of the Gas Pressure at the Time of Muzzle Clearance.

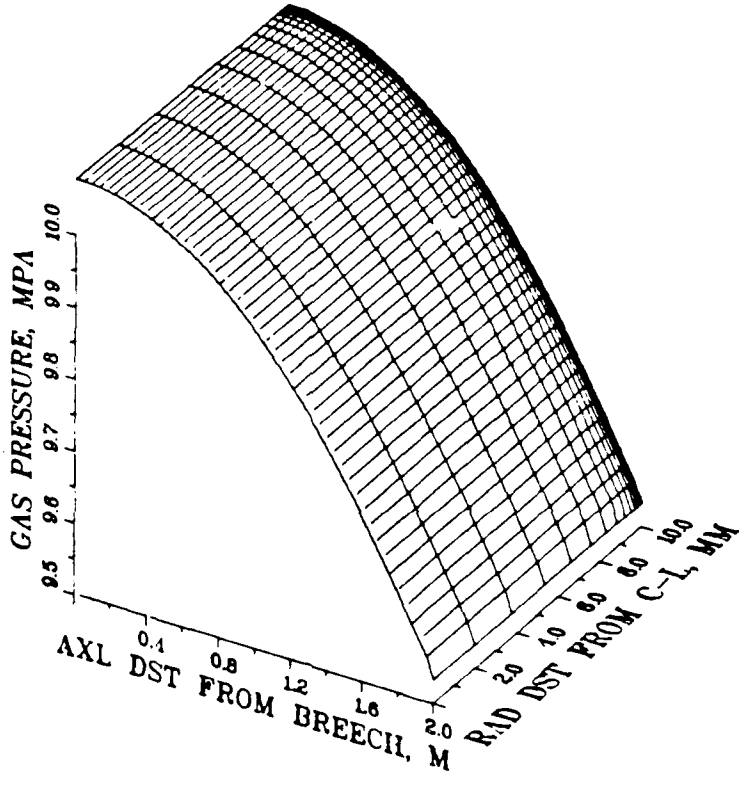

Figure 9. Lagrange Gun, Laminar Flow, Adiabatic Walls: Spatial Distribution of the Gas Pressure at the Time of Muzzle Clearance.

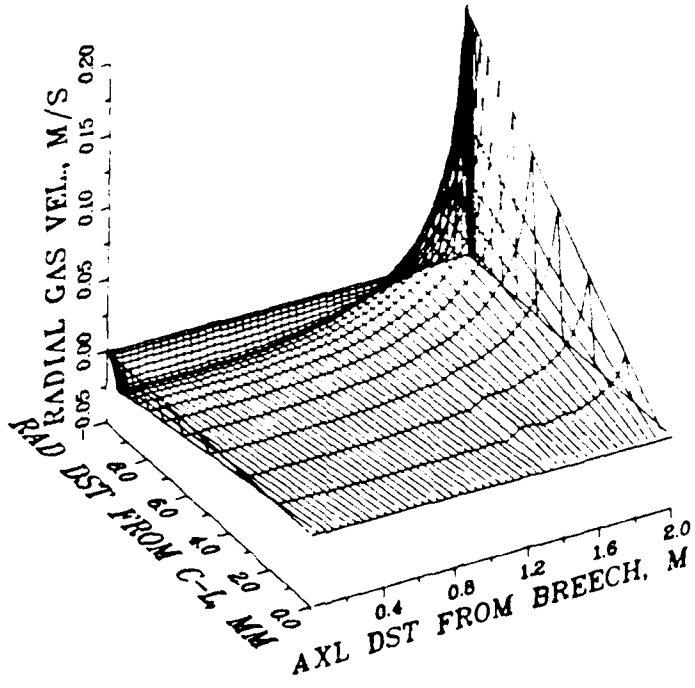

Figure 10. Lagrange Gun, Laminar Flow, Adiabatic Walls: Spatial Distribution of the Radial Gas Velocity at the Time of Muzzle Clearance.

For the Lagrange gun considered above the Reynolds number based on the tube's diameter and muzzle velocity is of the order of 10^7. Therefore, the assumption of a laminar flow might not be realistic, and we examined in further calculations the effects of turbulence. In comparison to the laminar flow, several important differences were observed when the two algebraic turbulence models described in Section IV were applied. However, the difference between the effects of the two turbulence models was found to be insignificant. Therefore, we do not specify the type of model in the presented results. First, one observes a difference in the projectile performance between the laminar and turbulent type flows. This is shown in Figure 11 in terms of the pressure histories at the breech, in Figure 12 in terms of the temperature histories at the breech, and in Figure 13 in terms of the projectile velocity histories. In the turbulent flow simulation, the projectile muzzle velocity is about 50 m/s less than in the laminar flow simulation. The axial velocity flow field at the time of muzzle clearance is shown in Figure 14. The velocity boundary layer is fully developed between the center line and the tube wall. The axial velocity overshoots the projectile velocity near the center line. This overshoot is related to the radial gas velocity (Figure 15) which, near the projectile base, is one to two orders of magnitude larger than in the case of a laminar flow (Figure 10). In this region, the greater radial gas flux toward the tube wall transports mass away from center-line which in turn can accelerate the axial flow. The radial variation of the axial velocity (Figure 16), the radial velocity (Figure 17) and the temperature (Figure 18) taken 0.25 m upstream of the muzzle show some details of the differences between the laminar and turbulent flows at the time of muzzle clearance. Boundary layer calculations in Ref. 7 show comparable trends between laminar and turbulent flows. However, the flow patterns computed by different types of turbulence models, e.g., non-algebraic models, may differ. An experiment corresponding to this idealized expansion flow is needed to validate a turbulence model. Such experiments are being attempted at the French-German Institute (ISL) in France and the Ernst-Mach-Institut (EMI) in Germany.

In a second series of calculations we investigated the significance of heat transfer to the tube wall. The heating of the wall's surface has practical implications because it influences the erosion of the tube. Our heat transfer model together with the calculation of the heat conduction in the wall couples the unsteady behavior in both media, and it is discussed in Section III. We now show results obtained for the laminar Lagrange gun expansion flow with heat transfer from the gas to the tube wall. Initially the wall is assumed to be at ambient temperature. The thermal properties of the gun barrel are characterized by the barrel material density $\rho_w = 7.8$ kg/m^3, thermal conductivity $\lambda_w = 43$ W/(m K) and specific heat $c_w = 460$ J/(kg K). The pressure and temperature histories at the breech, and projectile velocity history are given in Figures 11-13, and can be compared with the other two simulations. The spatial profile of the axial velocity, radial velocity, pressure and temperature are plotted in Figures 19-22, respectively, at the time of muzzle clearance. Comparing the results to those of the laminar flow with adiabatic walls, we find that the velocity boundary layer as well as the temperature boundary layer are in the present case thinner, that the radial

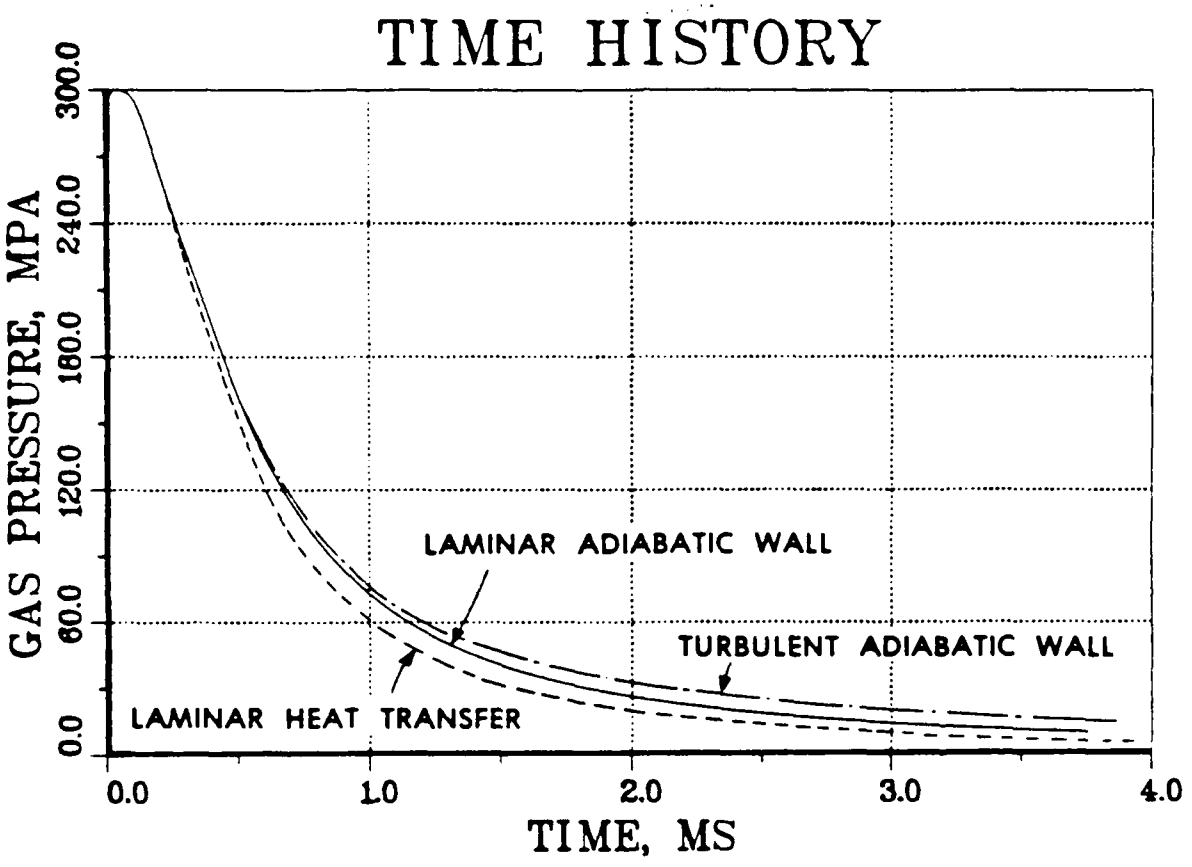

Figure 11. Lagrange Gun: Pressure Histories at the Center of the Breech for Both Laminar and Turbulent Flows with Adiabatic Walls, and for Laminar Flow with Heat Transfer.

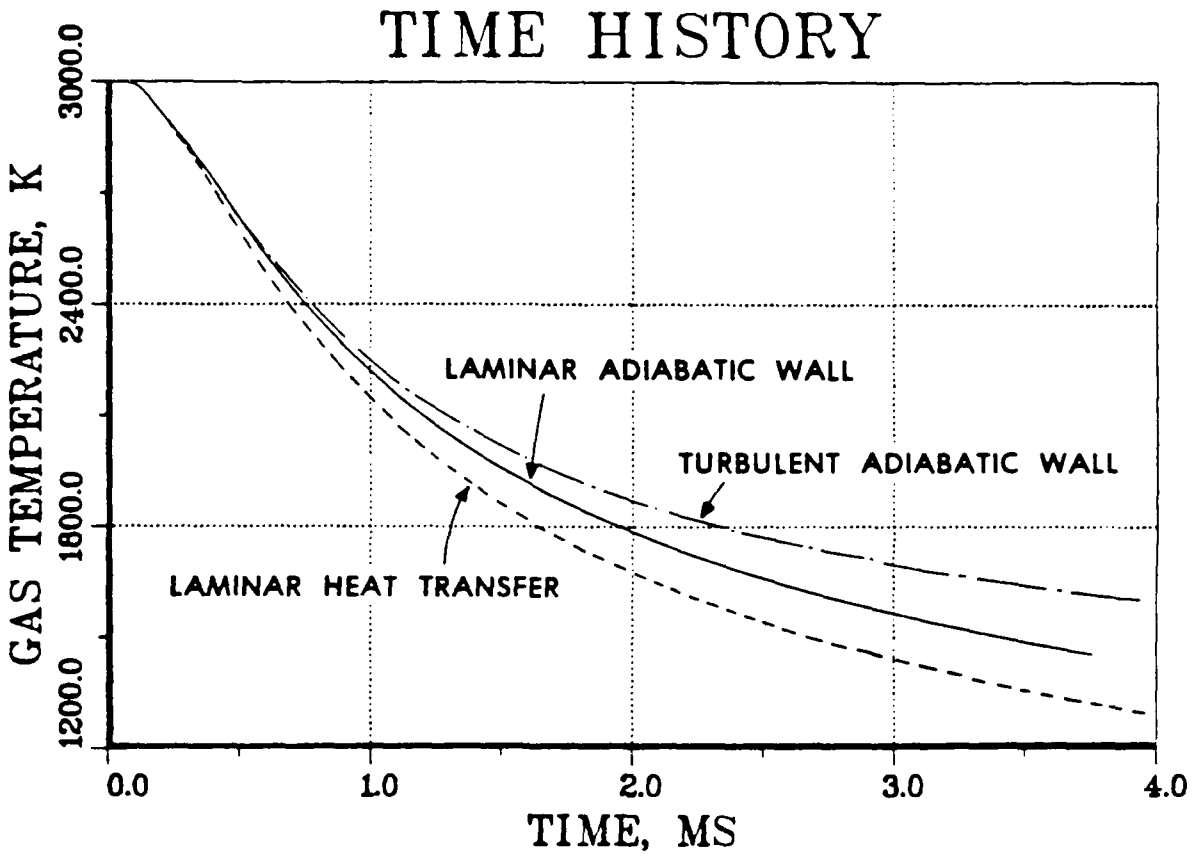

Figure 12. Lagrange Gun: Temperature Histories at the Center of the Breech for Both Laminar and Turbulent Flows with Adiabatic Walls, and for Laminar Flow with Heat Transfer.

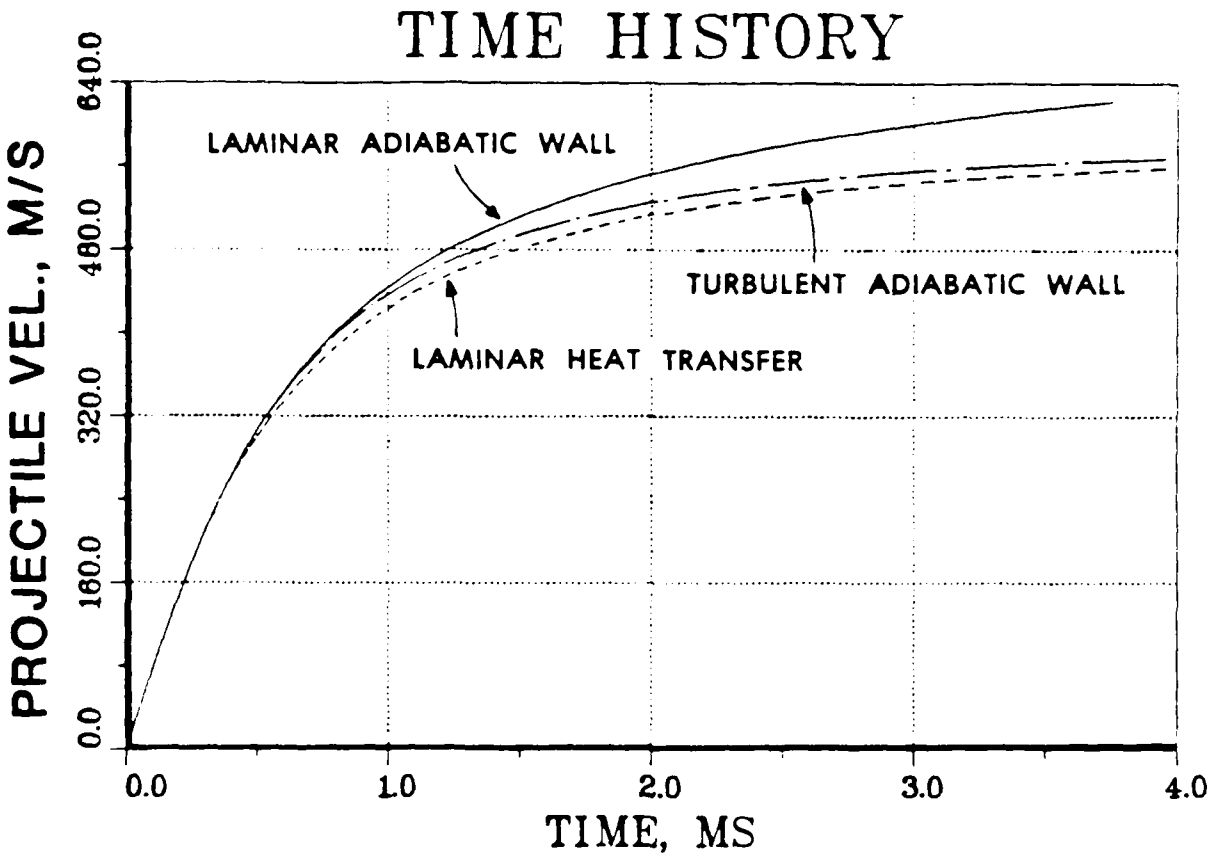

Figure 13. Lagrange Gun: Projectile Velocity Histories for Both Laminar and Turbulent Flows with Adiabatic Walls and for Laminar Flow with Transfer.

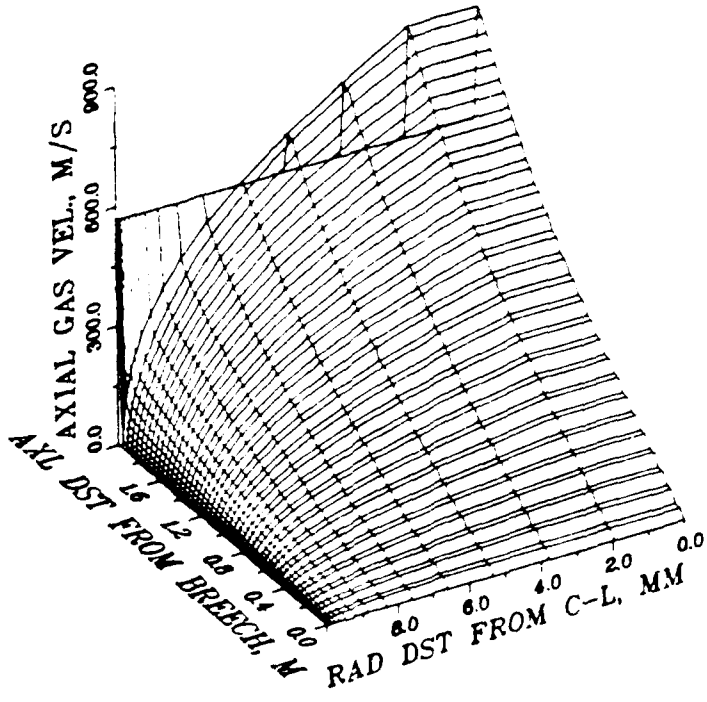

Figure 14. Lagrange Gun, Turbulent Flow, Adiabatic Walls: Spatial Distribution of the Axial Gas Velocity at the Time of Muzzle Clearance.

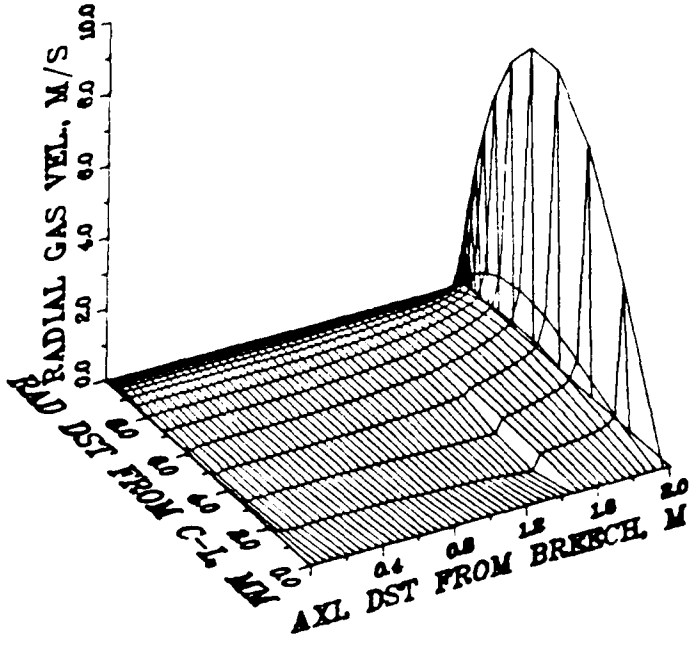

Figure 15. Lagrange Gun, Turbulent Flow, Adiabatic Walls: Spatial Distribution of the Radial Gas Velocity at the Time of Muzzle Clearance.

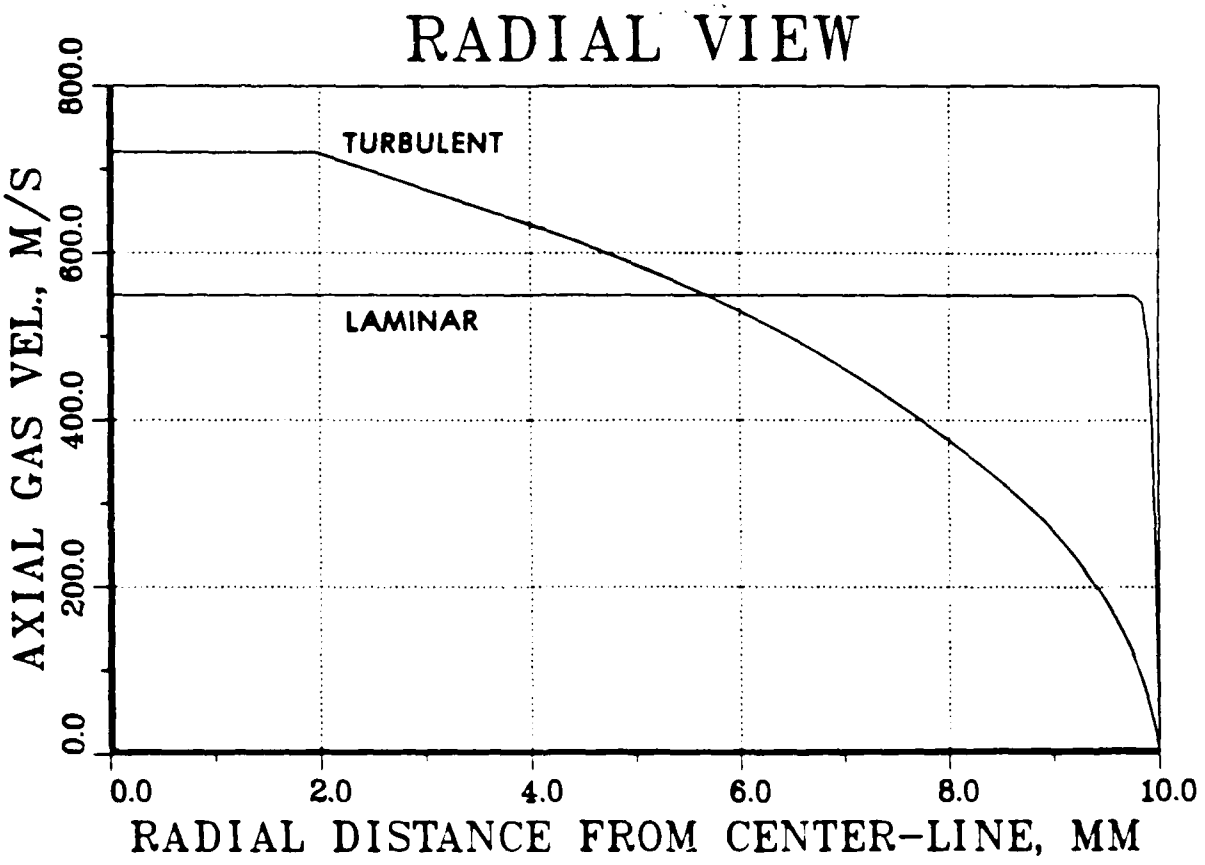

Figure 16. Lagrange Gun, Adiabatic Walls: Radial Profiles of the Axial Gas Velocity for Both Laminar and Turbulent Flow at the Time of Muzzle Clearance at 0.25 m Away from the Muzzle.

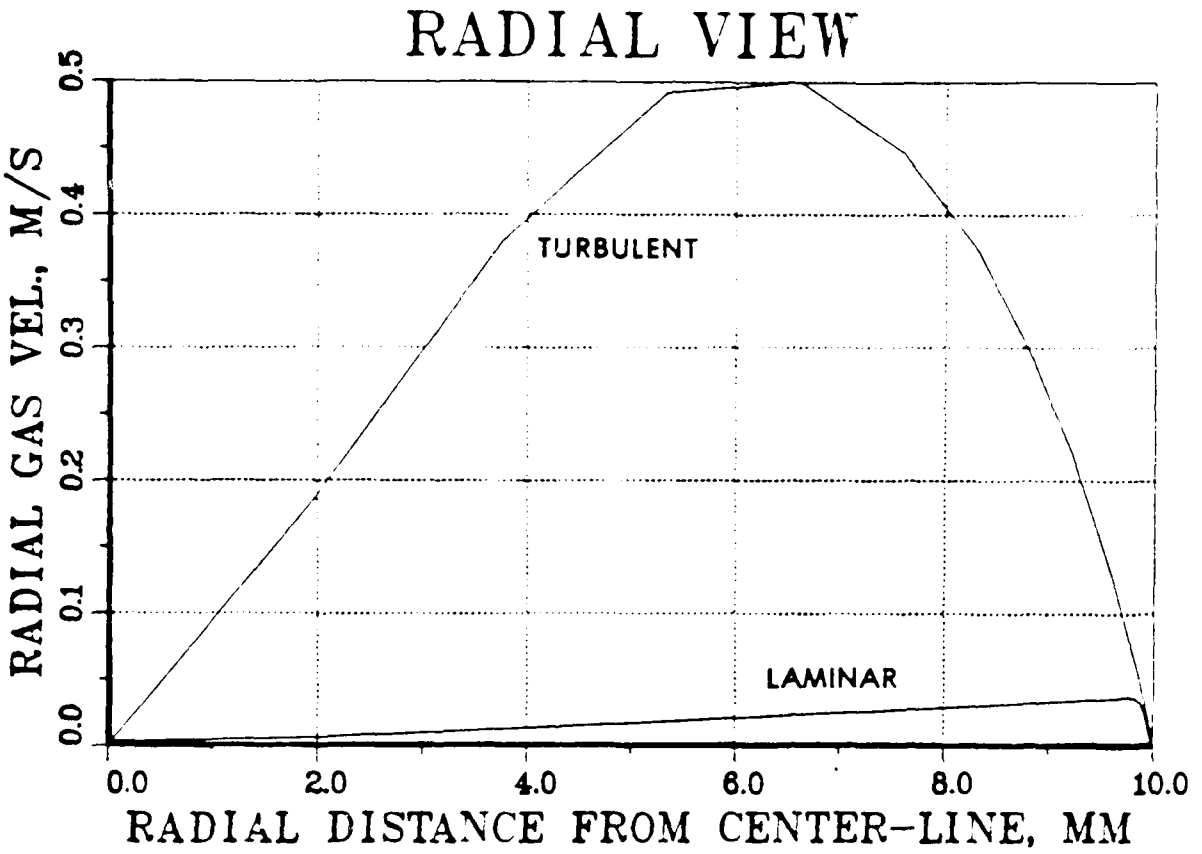

Figure 17. Lagrange Gun, Adiabatic Walls: Radial Profiles of the Radial Gas Velocity for Both Laminar and Turbulent Flow at the Time of Muzzle Clearance at 0.25 m Away from the Muzzle.

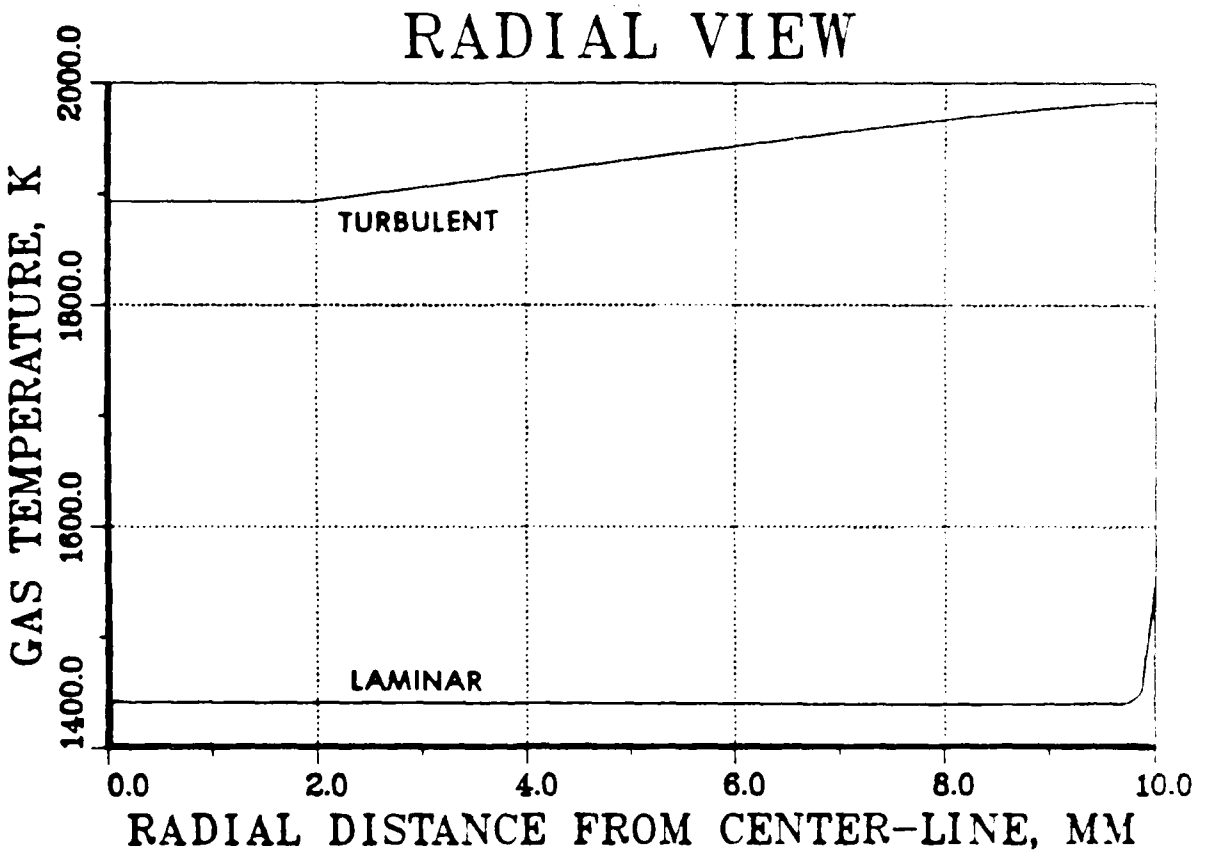

Figure 18. Lagrange Gun, Adiabatic Walls: Radial Profiles of the Gas Temperature for Both Laminar and Turbulent Flows at the Time of Muzzle Clearance at 0.25 m Away from the Muzzle.

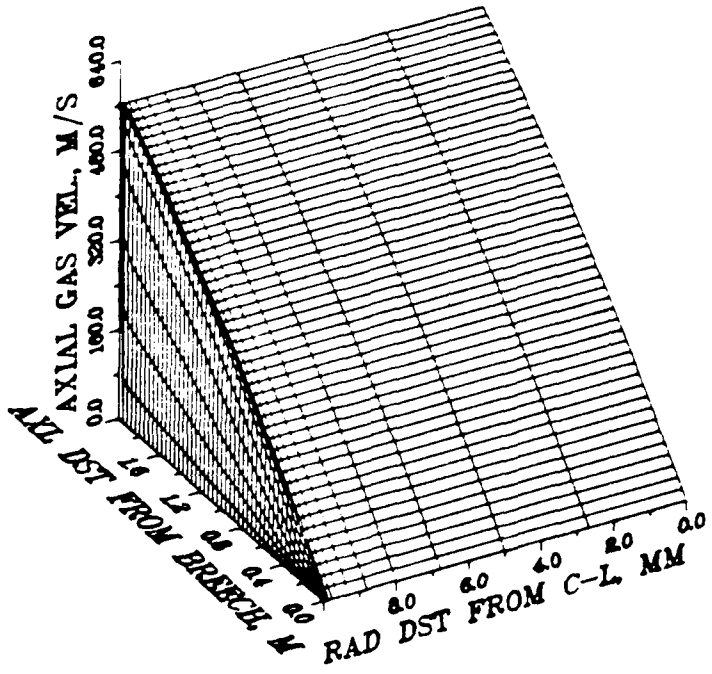

Figure 19. Lagrange Gun, Laminar Flow, Heat Transfer: Spatial Profile of the Axial Gas Velocity at the Time of Muzzle Clearance.

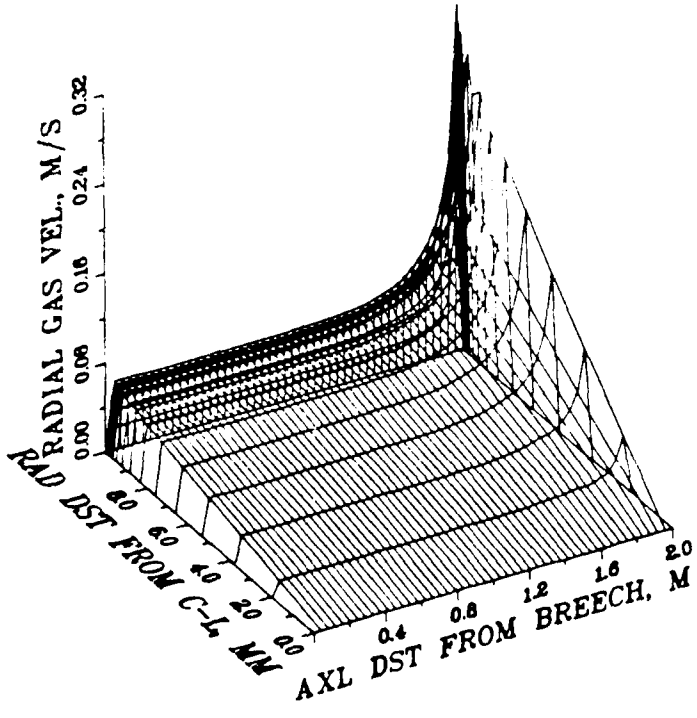

Figure 20. Lagrange Gun, Laminar Flow, Heat Transfer: Spatial Profile of the Radial Gas Velocity at the Time of Muzzle Clearance.

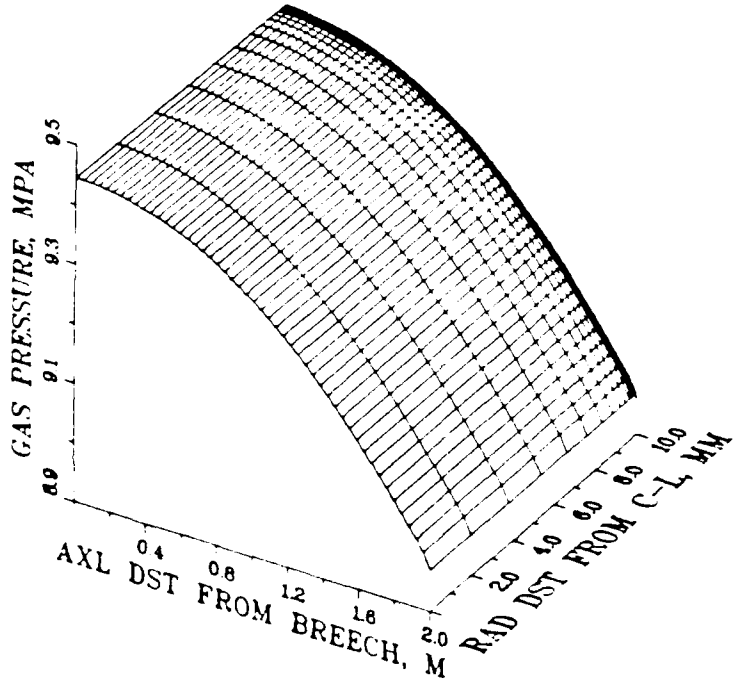

Figure 21. Lagrange Gun, Laminar Flow, Heat Transfer: Spatial Profile of the Gas Pressure at the Time of Muzzle Clearance.

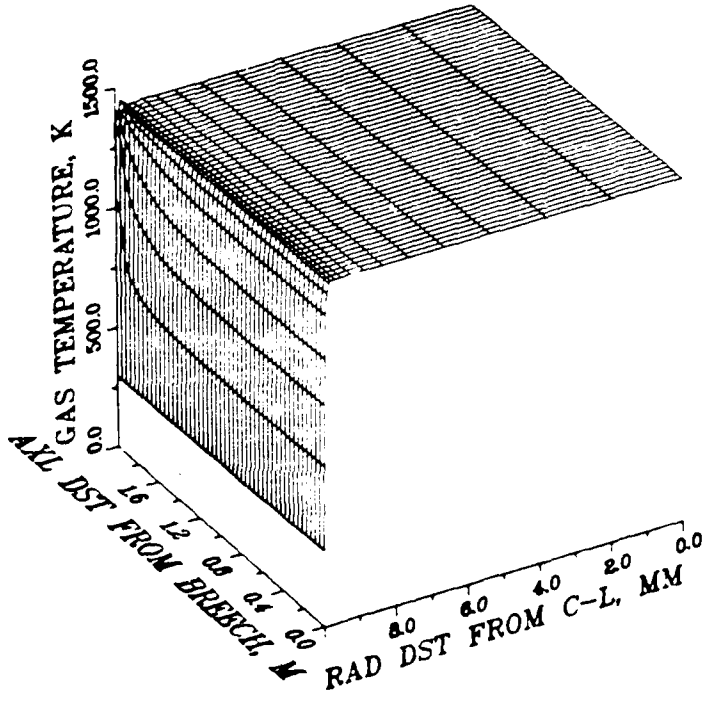

Figure 22. Lagrange Gun, Laminar Flow, Heat Transfer: Spatial Profile of the Gas Temperature at the Time of Muzzle Clearance.

velocity is about one order of magnitude higher, and that the radial velocity is always directed toward the wall. For example, the velocity boundary layer is only about 0.05 mm thick. Detailed comparisons across the boundary layer regions for axial velocities and temperatures are presented in Figures 23 and 24, and across the tube cross-section for the radial velocities are shown in Figure 25. All these profiles are at 0.25 m from the muzzle at the time of muzzle clearance. Figure 26 shows the history of the wall surface temperature at two different locations along the tube wall. One is taken at 150 mm away from the breech. This wall point belongs to the chamber, and is heated up from the beginning of the flow cycle. The second wall point is 250 mm away from the breech, and is heated up only after the projectile has passed it (at 0.47 ms). The maximum wall temperature occurs early in the 4 ms cycle. The laminar gas layer close to the tube wall cools rapidly because the transport of heat in the tube wall by conduction is much faster than the transport of heat by conduction and convection on the gas side towards the wall. To obtain the heat transfer precisely from the gas to the wall, we need to compute the radial temperature gradient on both sides of the inner bore surface as accurately as possible. The temperature boundary layer, however, is very thin as it is shown in Figures 22 and 24. This implies that very small grid sizes must be used close to the wall. The smallest one in radial direction for Figure 26 is 0.73 μm .

The final simulations are of one-phase flows in the real gun, i.e., of a gas flow with mass and energy sources. The pressure and temperature histories at the breech and projectile, and the projectile velocity and displacement histories for the laminar flow simulation and for the real gun are given in Figures 2-5. Figures 27-40 are a series of three-dimensional profiles which characterize both the laminar and turbulent flows inside an adiabatic tube. The group of figures associated with the laminar flow are at two times: the first at 3.6 ms when maximum pressure is achieved and the second at 5.3 ms when the projectile exits the tube. For these calculations a nonuniform radial grid is used with the minimum grid size of 0.73 μm because of the thinness of the boundary layer. We excluded the profile of the radial velocity at 3.6 ms because the magnitude of this component was smaller than 0.05 m/s. Three-dimensional profiles show the turbulent flow fields when maximum pressure occurs at 3.6 ms (Figures 34-37), and when the projectile exits the tube at 5.49 ms (Figures 38-40). As in the Lagrange gun, the differences are minimal between the simulations with different turbulence model, but significant between the laminar and turbulence simulations.

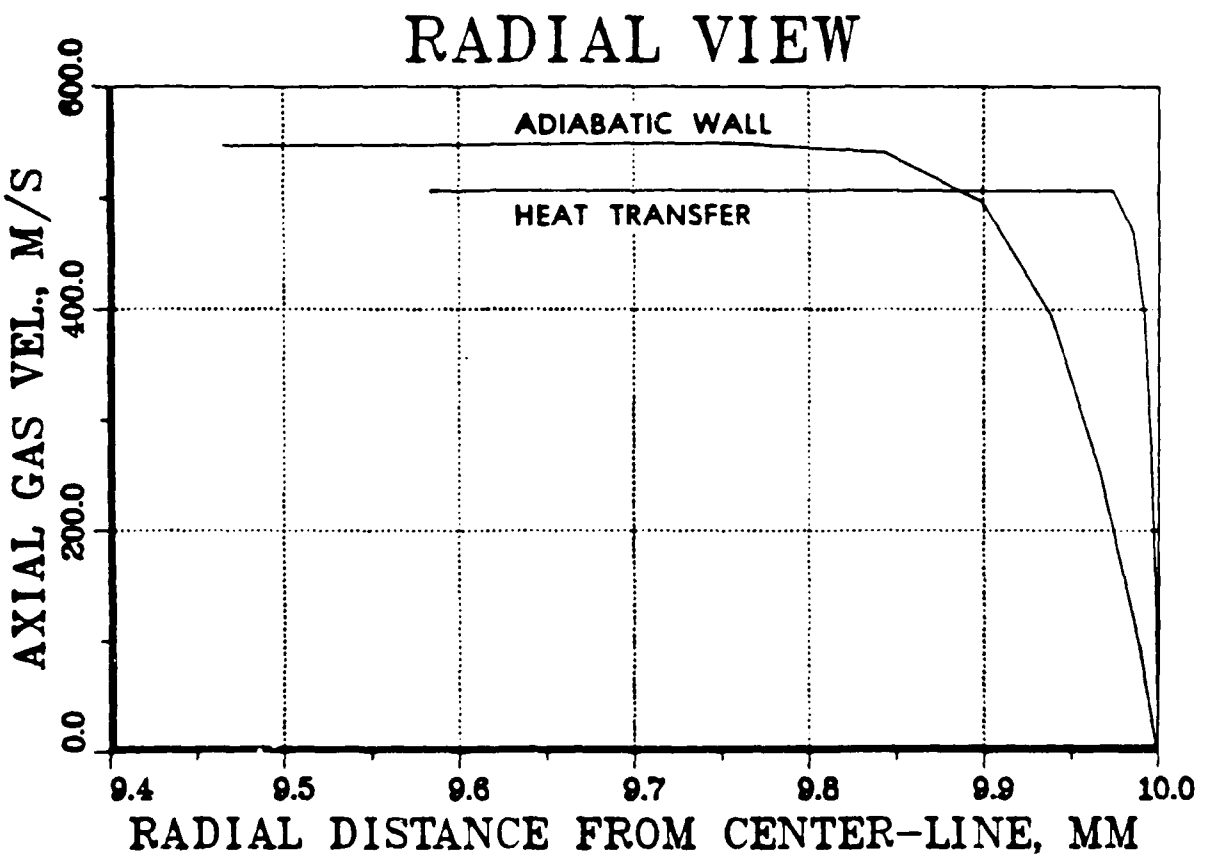

Figure 23. Lagrange Gun, Laminar Flow: Radial Profiles of the Axial Gas Velocity for Adiabatic and Heat Permeable Walls at the Time of Muzzle Clearance 0.25 m Away from the Muzzle.

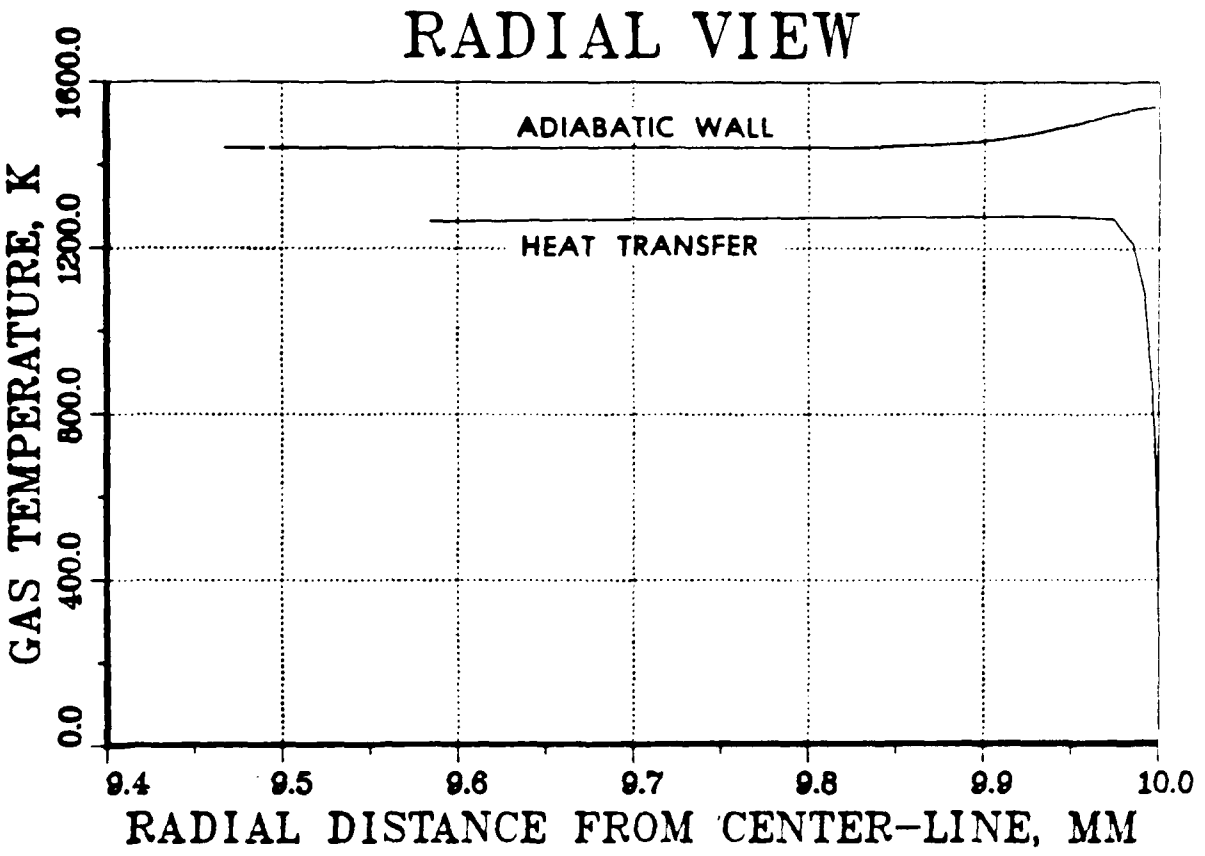

Figure 24. Lagrange Gun, Laminar Flow: Radial Profiles of the Gas Temperature for Adiabatic and Heat Permeable Walls at the Time of Muzzle Clearance 0.25 m Away from the Muzzle.

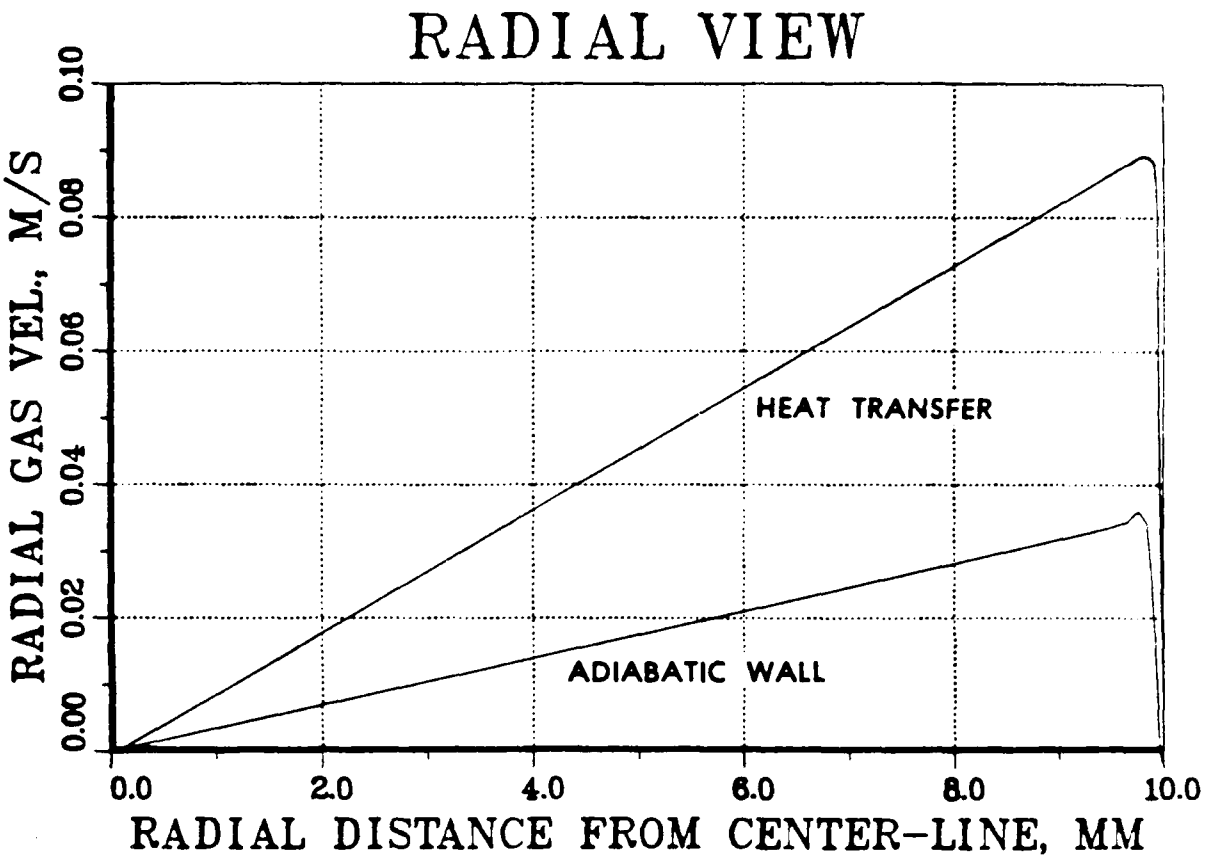

Figure 25. Lagrange Gun, Laminar Flow: Radial Profiles of the Radial Gas Velocity for Adiabatic and Heat Permeable Walls at the Time of Muzzle Clearance 0.25 m Away from the Muzzle.

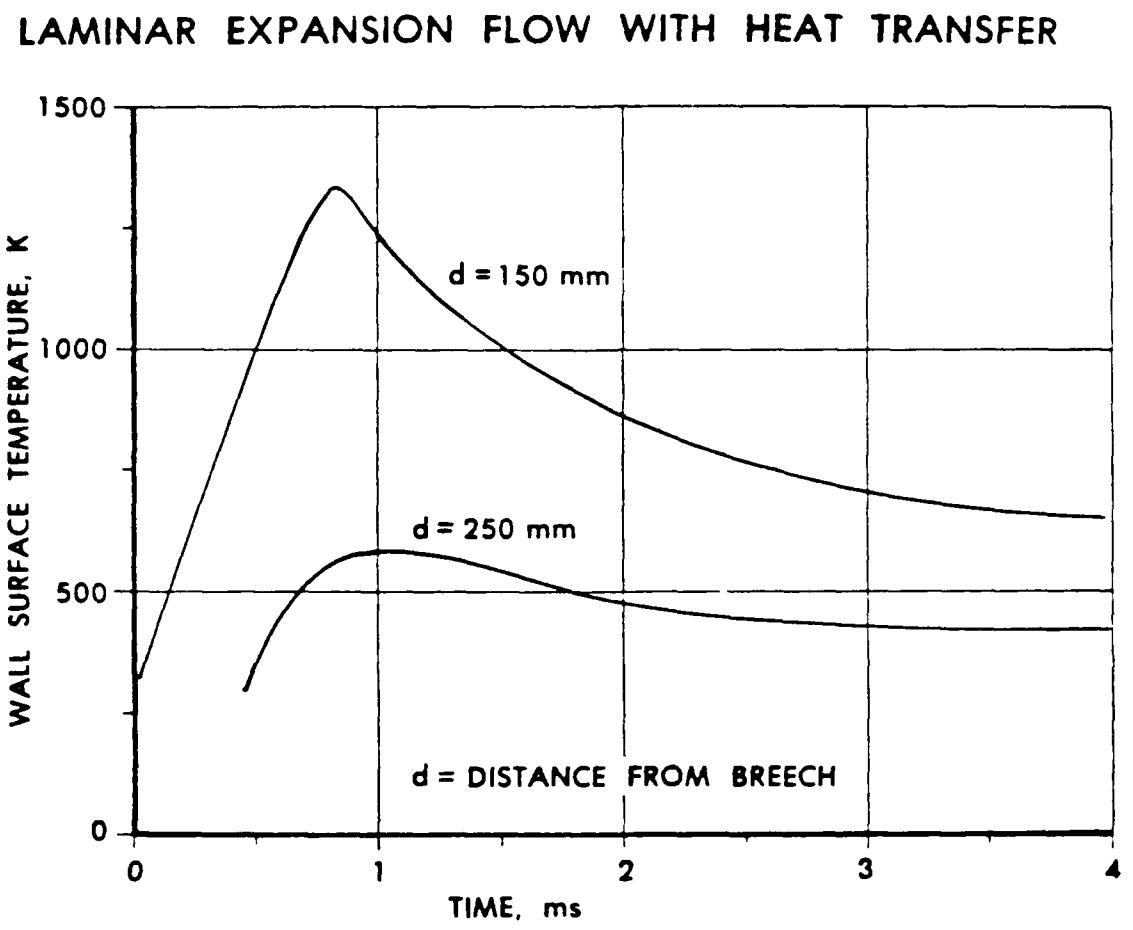

Figure 26. History of the Wall Surface Temperature for a Laminar Expansion Flow (LG) with Heat Transfer to the Tube Wall at the Locations 150 mm (inside the chamber) and 250 mm (inside the barrel) Away from the Breech.

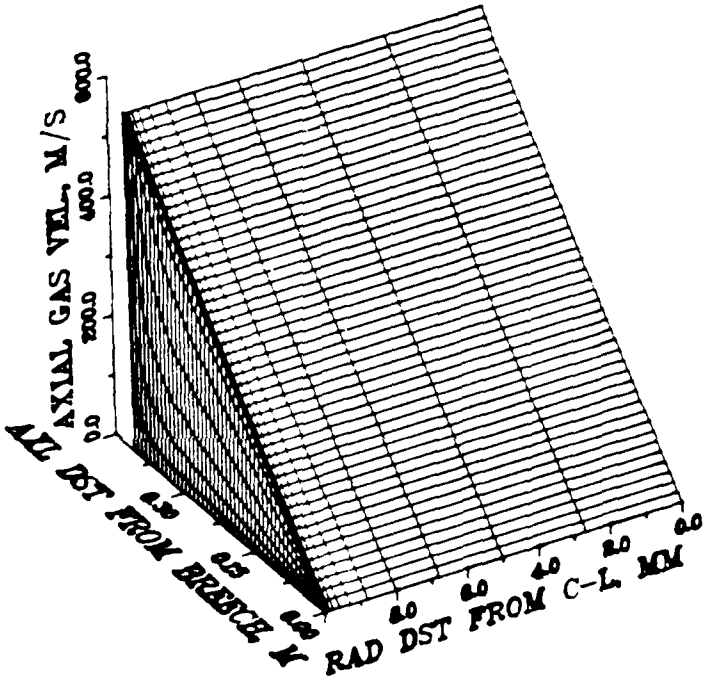

Figure 27. Real Gun, Laminar Flow, Adiabatic Walls: Spatial Distribution of the Axial Gas Velocity at 3.6 ms.

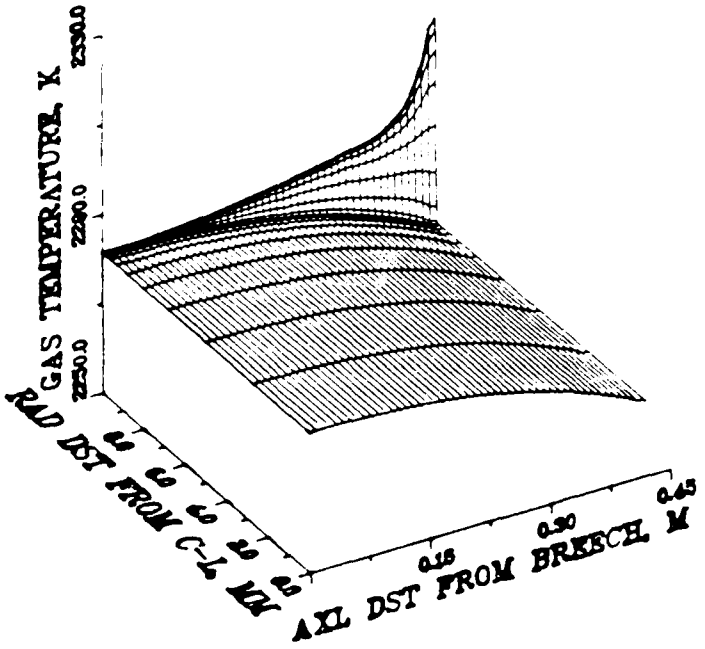

Figure 28. Real Gun, Laminar Flow, Adiabatic Walls: Spatial Distribution of the Gas Temperature at 3.0 ms.

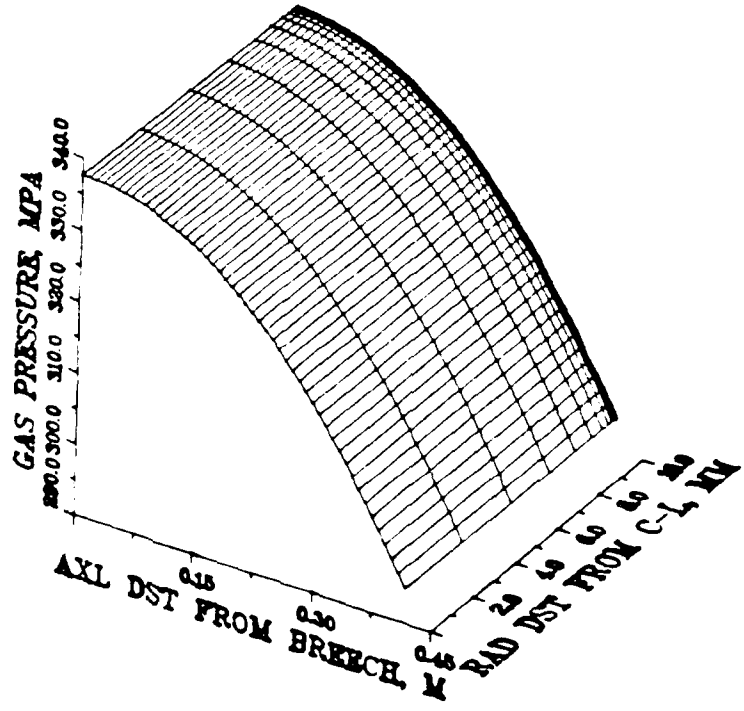

Figure 29. Real Gun, Laminar Flow, Adiabatic Walls: Spatial Distribution of the Gas Pressure at 3.6 ms.

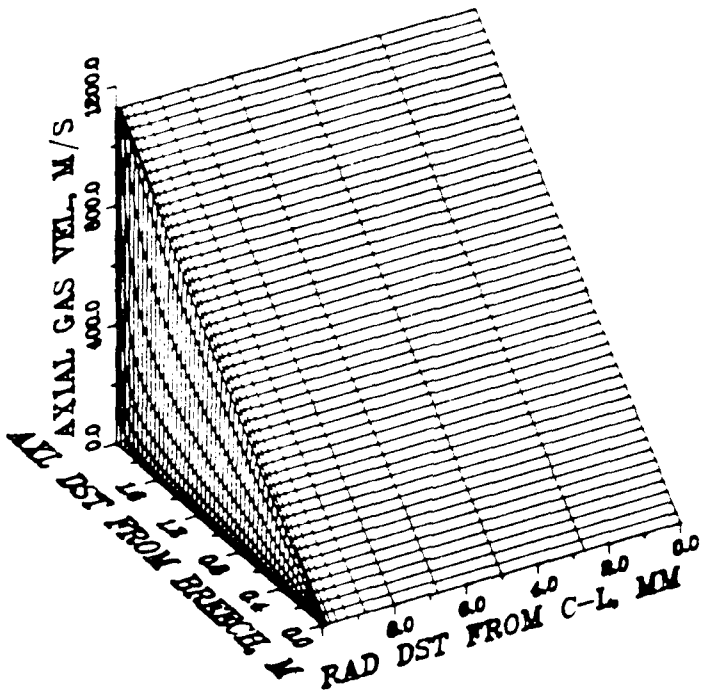

Figure 30. Real Gun, Laminar Flow, Adiabatic Walls: Spatial Distribution of the Axial Gas Velocity at Muzzle Clearance (5.3 ms).

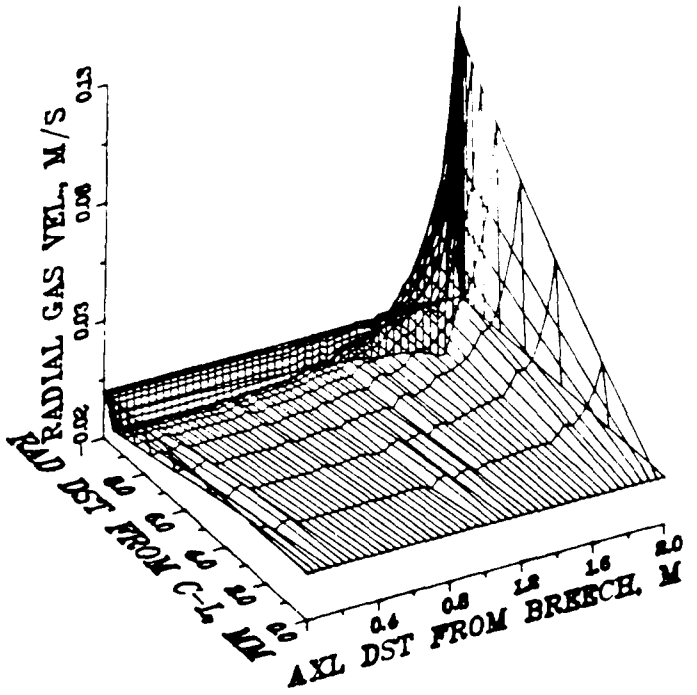

Figure 31. Real Gun, Laminar Flow, Adiabatic Walls: Spatial Distribution of the Radial Gas Velocity at Muzzle Clearance (5.3 ms).

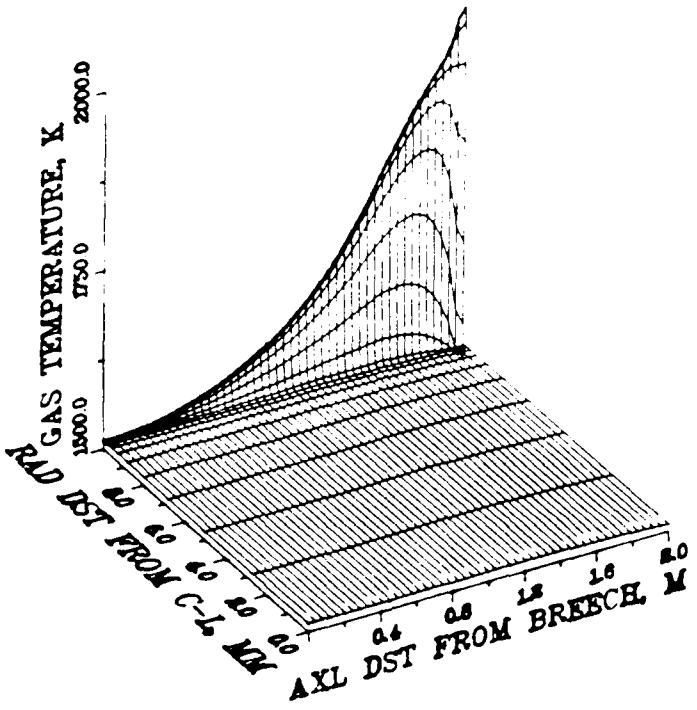

Figure 32. Real Gun, Laminar Flow, Adiabatic Walls: Spatial Distribution of the Gas Temperature at Muzzle Clearance (5.3 ms).

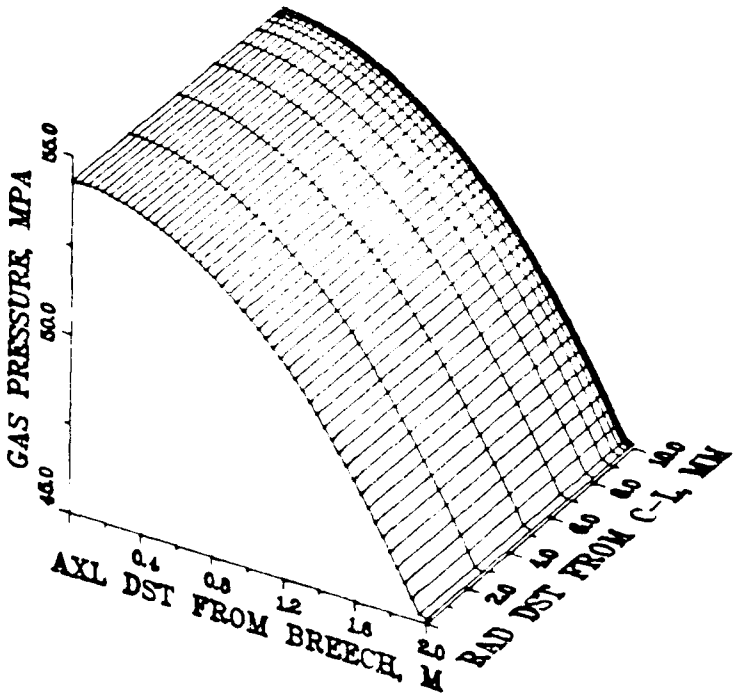

Figure 33. Real Gun, Viscous Flow, Adiabatic Walls: Spatial Distribution of the Gas Pressure at Muzzle Clearance (5.3 ms).

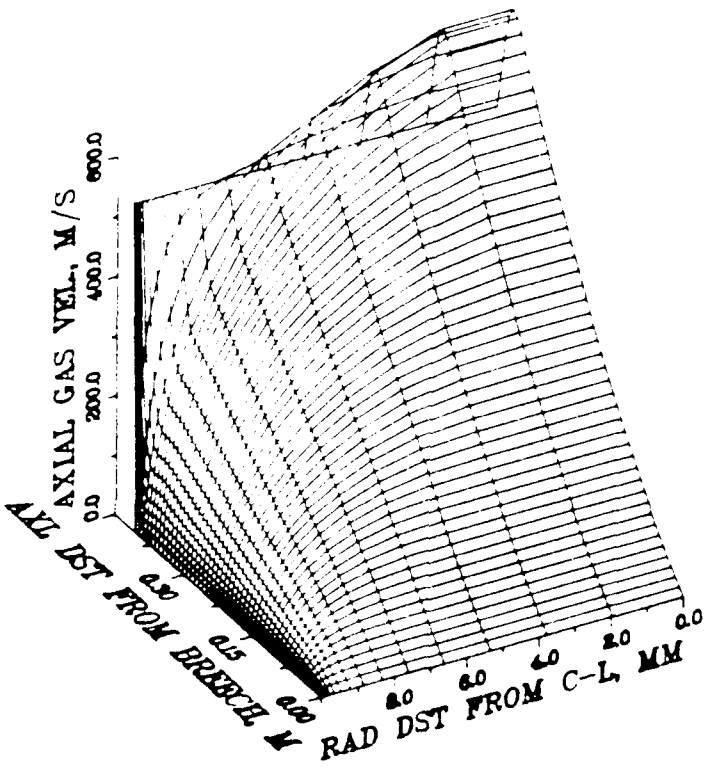

Figure 34. Real Gun, Turbulent Flow, Adiabatic Walls: Spatial Distribution of the Axial Gas Velocity at 3.6 ms.

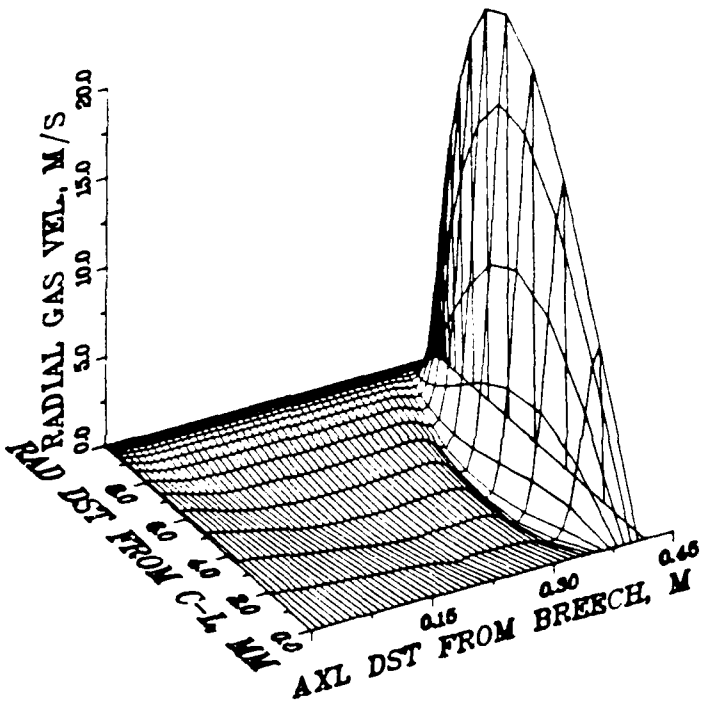

Figure 35. Real Gun, Turbulent Flow, Adiabatic Walls: Spatial Distribution of the Radial Gas Velocity at 3.6 ms.

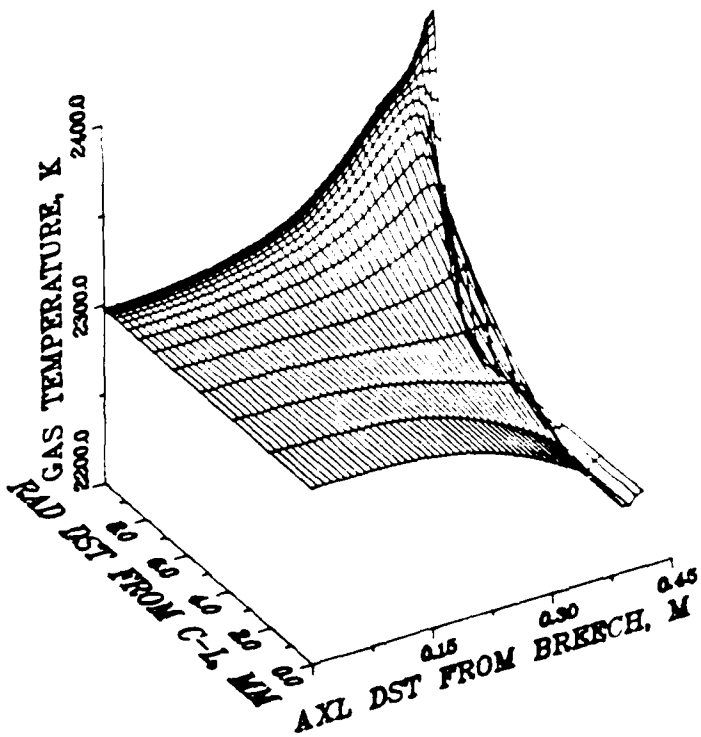

Figure 36. Real Gun, Turbulent Flow, Adiabatic Walls: Spatial Distribution of the Gas Temperature at 3.6 ms.

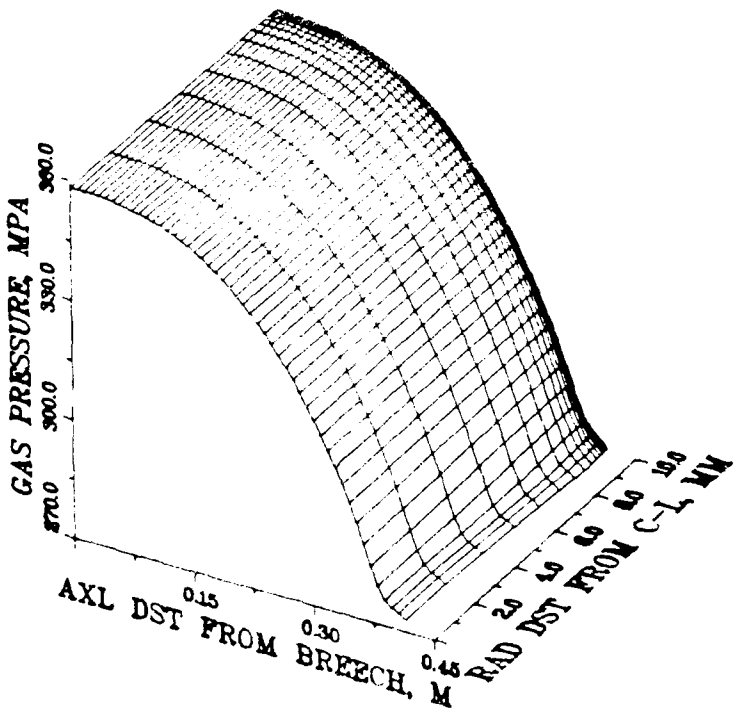

Figure 37. Real Gas, Turbulent Flow, Adiabatic Walls: Spatial Distribution of the Gas Pressure at 3.6 ms.

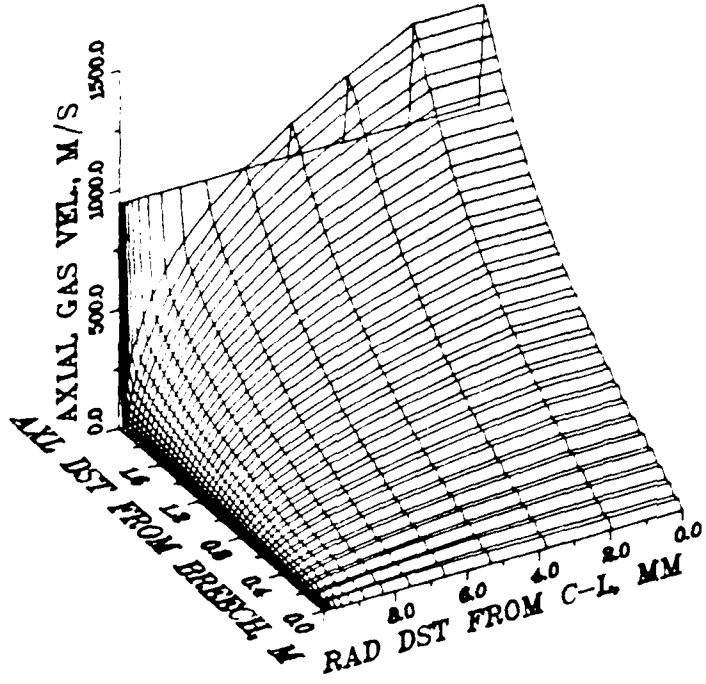

Figure 38. Real Gun, Turbulent Flow, Adiabatic Walls: Spatial Distribution of the Axial Gas Velocity at Muzzle Clearance (5.49 ms).

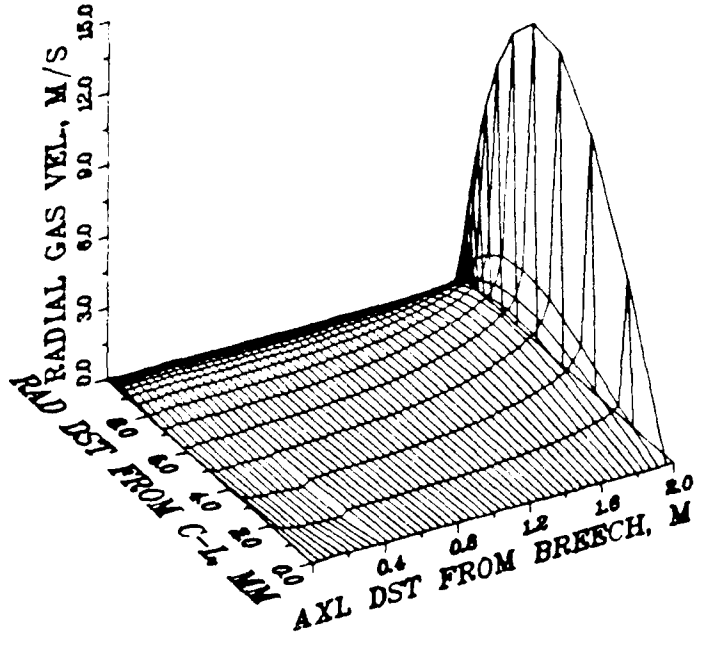

Figure 39. Real Gun, Turbulent Flow, Adiabatic Walls: Spatial Distribution of the Radial Gas Velocity at Muzzle Clearance (5.49 ms).

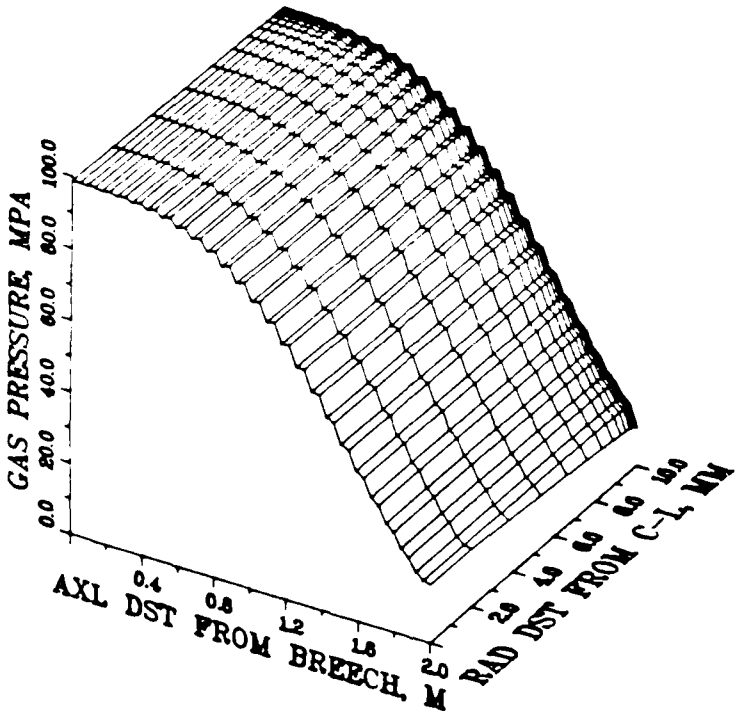

Figure 40. Real Gun, Turbulent Flow, Adiabatic Walls: Spatial Distribution of the Gas Pressure at Muzzle Clearance (5.49 ms).

VI. SUMMARY

Special interior ballistic phenomena are investigated by using the DELTA computer code, which is designed to calculate the multidimensional, two-phase flow behind an accelerating projectile inside a gun tube. Details of the heat transfer and turbulence submodels used in the simulations are given in this report. The general mathematical model and numerical algorithm are described in a companion paper, Ref. 3. Results are given for two types of idealized, one-phase interior ballistics gun simulations: a pure expansion flow, and a flow with moving mass and heat sources. Comparisons are made between laminar and turbulent flows as well as between flows in an adiabatic tube and in a tube that allows heat transfer. The comparisons show that the flow structure and the motion of the projectile are both significantly influenced by turbulence and heat conduction, because of a strong coupling between the core flow and boundary phenomena. A study of the effects of turbulence and heat conduction therefore can be best accomplished with a multi-dimensional mathematical model, such as the DELTA code.

REFERENCES

1. "Fluid Dynamics Aspects of Internal Ballistics," AGARD Advisory Report No. 172, 1982.

2. Celmins, A.K.R., Schmitt, J.A., "Three-Dimensional Modeling of Gas-Combusting Solid Two-Phase Flows, "Multi-Phase Flow and Heat Transfer III, Part B: Applications, T. N. Veziroglu and A.E. Bergles, editors, pp. 681-698, Elsevier Science Publishers, Amsterdam, 1984

3. Schmitt, J.A., "A Numerical Algorithm for the Multidimensional, Multiphase, Viscous Equations of Interior Ballistics," Transactions of the Second Army Conference on Applied Mathematics and Computing, ARO-Report 85-1, pp. 649-691, 1985

4. Shelton, S., Bergles, A., Sana, P., "Study of Heat Transfer and Erosion in Gun Barrels," Air Force Armament Laboratory, Eglin Air Force Base, Florida, AFATL-TR-73-69, 1973.

5. Gough, P., "Modeling of Rigidized Gun Propelling Charges," Ballistic Research Laboratory, Aberdeen Proving Ground, Maryland ARBRL-CR-00518, 1983.

6. Nelson, C.W., Ward, J.R., "Calculation of Heat Transfer to the Gun Barrel Wall," J. Ballistics 6 (3), pp. 1518-1524, 1982.

7. Barlett, E.P., Anderson, L.W., Kendall, R.M., "Time-Dependent Boundary Layers with Application to Gun Barrel Heat Transfer," Proceedings 1972 Heat Transfer Fluid Mech. Institute, Stanford University, CA, 1972.

8. Buckingham, A.C., "Modeling Propellant Combustion Interacting with an Eroding Solid Surface," Lawrence Livermore Laboratory, UCRL-83727, 1980.

9. Adams, M.J., Krier, H., "Unsteady Internal Boundary Layer Analysis Applied to Gun Barrel Wall Heat Transfer," Int. J. Heat Mass Transfer, Vol. 24, No. 12, pp. 1925-1935, 1981.

10. Aerospace Structural Metal Handbook, "Ferrous Alloys," 1973.

11. Schlichting, H., "Boundary Layer Theory," McGraw-Hill, 1968.

12. Rubesin, M.W., "Numerical Turbulence Modeling," AGARD-LS-86.

13. Kussoy, M.I., Viegas, J.R., Horstman, C.C., "Investigation of a Three-Dimensional Shock Wave Separated Turbulent Boundary Layer," AIAA J., Vol. 18 (1980), No. 12, pp. 1477.

14. Heiser, R., Hensel, D., "AMI: Ein Achsensymmetrisches Modell der Innenballistik, Teil 1: Laminare Einphasenströmung ohne Wärmeübergang (AMI: An Axisymmetric Model of Interior Ballistics, Part 1: Laminar One-Phase Flow without Heat Transfer)," Fraunhofer-Institut für Kurzzeitdynamik, Ernst-Mach-Institut, Abteilung für Ballistik, Weil am Rhein, FRG, Report No. 4/80, 1980.

15. Heiser, R., Hensel, D., "Berechnung der Gasströmung in einem Waffenrohr mit Hilfe des zweidimensionalen AMI-Modells (Calculation of the Gas Flow Inside a Gun Tube Using the Two-Dimensional AMI Model)," Fraunhofer-Institut für Kurzzeitdynamik, Ernst-Mach-Institut, Abteilung für Ballistik, Weil am Rhein, FRG, Report No. E 1/81, 1981.

DISTRIBUTION LIST

No. Of Copies	Organization
12	Administrator Defense Technical Info Center ATTN: DTIC-DDA Cameron Station Alexandria, VA 22304-6145
1	Commander USA Concepts Analysis Agency ATTN: D. Hardison 8120 Woodmont Avenue Bethesda, MD 20014-2797
1	HQDA/DAMA-ZA Washington, DC 20310-2500
1	HQDA, DAMA-CSM, E. Lippi Washington, DC 20310-2500
1	HQDA/SARDA Washington, DC 20310-2500
1	Commander US Army War College ATTN: Library-FF229 Carlisle Barracks, PA 17013
1	US Army Ballistic Missile Defense Systems Command Advanced Technology Center P. O. Box 1500 Huntsville, AL 35807-3801
1	Chairman DOD Explosives Safety Board Room 856-C Hoffman Bldg. 1 2461 Eisenhower Avenue Alexandria, VA 22331-9999
1	Commander US Army Materiel Command ATTN: AMCPM-GCM-WF 5001 Eisenhower Avenue Alexandria, VA 22333-5001
1	Commander US Army Materiel Command ATTN: AMCDRA-ST 5001 Eisenhower Avenue Alexandria, VA 22333-5001
1	Commander US Army Materiel Command ATTN: AMCDE-DW 5001 Eisenhower Avenue Alexandria, VA 22333-5001
5	Project Manager Cannon Artillery Weapons System, ARDC, AMCCOM ATTN: AMCPM-CW, F. Menke AMCPM-CWW AMCPM-CWS M. Fisette AMCPM-CWA R. DeKleine H. Hassmann Dover, NJ 07801-5001
2	Project Manager Munitions Production Base Modernization and Expansion ATTN: AMCPM-PBM, A. Siklosi AMCPM-PBM-E, L. Laibson Dover, NJ 07801-5001
3	Project Manager Tank Main Armament System ATTN: AMCPM-TMA, K. Russell AMCPM-TMA-105 AMCPM-TMA-120 Dover, NJ 07801-5001
1	Commander US Army Watervliet Arsenal ATTN: SARWV-RD, R. Thierry Watervliet, NY 12189-5001

DISTRIBUTION LIST

No. Of Copies	Organization
20	Commander US Army ARDC, AMCCOM ATTN: SMCAR-TSS SMCAR-TDC SMCAR-LC LTC N. Barron SMCAR-LCA A. Beardell D. Downs S. Einstein S. Westley S. Bernstein C. Roller J. Rutkowski SMCAR-LCB-I D. Spring SMCAR-LCE SMCAR-LCM-E S. Kaplowitz SMCAR-LCS SMCAR-LCU-CT E. Barrieres R. Davitt SMCAR-LCU-CV C. Mandala SMCAR-LCW-A M. Salsbury SMCAR-SCA L. Stiefel B. Brodman Dover, NJ 07801-5001
4	Commander US Army Armament Munitions and Chemical Command ATTN: SMCAR-ESP-L Rock Island, IL 61299-7300
1	HQDA DAMA-ART-M Washington, DC 20310-2500
1	Director Benet Weapons Laboratory Armament R&D Center US Army AMCCOM ATTN: SMCAR-LCB-TL Watervliet, NY 12189-5001
1	Commander US Army Aviation Research and Development Command ATTN: AMSAV-E 4300 Goodfellow Blvd. St. Louis, MO 63120-1702
1	Commander US Army TSARCOM 4300 Goodfellow Blvd. St. Louis, MO 63120-1702
1	Director US Army Air Mobility Research And Development Laboratory Ames Research Center Moffett Field, CA 94035-1099
1	Commander US Army Communications - Electronics Command ATTN: AMSEL-ED Fort Monmouth, NJ 07703-5301
1	Commander ERADCOM Technical Library ATTN: DELSD-L (Report Section) Fort Monmouth, NJ 07703-5301
1	Commander US Army Harry Diamond Lab. ATTN: DELHD-TA-L 2800 Powder Mill Road Adelphi, MD 20783-1145
1	Commander US Army Missile Command ATTN: AMSMI-CM Redstone Arsenal, AL 35898-5249

DISTRIBUTION LIST

No. Of Copies	Organization
1	Director US Army Missile and Space Intelligence Center ATTN: AIAMS-YDL Redstone Arsenal, AL 35898-5500
1	Commander US Army Missle Command Research, Development, and Engineering Center ATTN: AMSMI-RD Redstone Arsenal, AL 35898-5500
1	Commandant US Army Aviation School ATTN: Aviation Agency Fort Rucker, AL 36360
1	Commander US Army Tank Automotive Command ATTN: AMSTA-TSL Warren, MI 48092-2498
1	Commander US Army Tank Automotive Command ATTN: AMSTA-CG Warren, MI 48092-2498
1	Project Manager Improved TOW Vehicle ATTN: AMCPM-ITV US Army Tank Automotive Command Warren, MI 48092-2498
2	Program Manager M1 Abrams Tank System ATTN: AMCPM-GMC-SA, T. Dean Warren, MI 48092-2498
1	Project Manager Fighting Vehicle Systems ATTN: AMCPM-FVS Warren, MI 48092-2498
1	President US Army Armor & Engineer Board ATTN: ATZK-AD-S Fort Knox, KY 40121-5200
1	Project Manager M-60 Tank Development ATTN: AMCPM-M60TD Warren, MI 48092-2498
1	Director US Army TRADOC Systems Analysis Activity ATTN: ATAA-SL White Sands Missile Range, NM 88002
1	Commander US Army Training & Doctrine Command ATTN: ATCD-MA/ MAJ Williams Fort Monroe, VA 23651
2	Commander US Army Materials Technology Laboratory (MLT) ATTN: AMXMR-ATL Tech Library Watertown, MA 02172
1	Commander US Army Research Office ATTN: Tech Library P. O. Box 12211 Research Triangle Park, NC 27709-2211
1	Commander US Army Belvoir Research & Development Center ATTN: STRBE-WC Fort Belvoir, VA 22060-5606

DISTRIBUTION LIST

No. Of Copies	Organization
1	Commander US Army Logistics Mgmt Ctr Defense Logistics Studies Fort Lee, VA 23801
1	Commandant US Army Infantry School ATTN: ATSH-CD-CSO-OR Fort Benning, GA 31905
1	President US Army Artillery Board Ft. Sill, OK 73503-5600
1	Commandant US Army Command and General Staff College Fort Leavenworth, KS 66027
1	Commandant US Army Special Warfare School ATTN: Rev & Tng Lit Div Fort Bragg, NC 28307
3	Commander Radford Army Ammunition Plant ATTN: SMCRA-QA/HI LIB Radford, VA 24141-0298
1	Commander US Army Foreign Science & Technology Center ATTN: AMXST-MC-3 220 Seventh Street, NE Charlottesville, VA 22901-5396
2	Commandant US Army Field Artillery Center & School ATTN: ATSF-CO-MW, B. Willis Ft. Sill, OK 73503-5600
1	Commander US Army Development and Employment Agency ATTN: MODE-TED-SAB Fort Lewis, WA 98433-5099
1	Chief of Naval Material Department of Navy ATTN: J. Amlie Arlington, VA 20360
1	Office of Naval Research ATTN: Code 473, R. S. Miller 800 N. Quincy Street Arlington, VA 22217-9999
3	Commandant US Army Armor School ATTN: ATZK-CD-MS M. Falkovitch Armor Agency Fort Knox, KY 40121-5215
2	Commander Naval Sea Systems Command ATTN: SEA 62R SEA 64 Washington, DC 20362-5101
1	Commander Naval Air Systems Command ATTN: AIR-954-Tech Lib Washington, DC 20360
1	Assistant Secretary of the Navy (R, E, and S) ATTN: R. Reichenbach Room 5E787 Pentagon Bldg. Washington, DC 20350
1	Naval Research Lab Tech Library Washington, DC 20375
5	Commander Naval Surface Weapons Center ATTN: Code G33, J. L. East W. Burrell J. Johndrow Code G23, D. McClure Code DX-21 Tech Lib Dahlgren, VA 22448-5000

DISTRIBUTION LIST

No. Of Copies	Organization
2	Commander US Naval Surface Weapons Center ATTN: J. P. Consaga C. Gotzmer Indian Head, MD 20640-5000
4	Commander Naval Surface Weapons Center ATTN: S. Jacobs/Code 240 Code 730 K. Kim/Code R-13 R. Bernecker Silver Springs, MD 20903-5000
2	Commanding Officer Naval Underwater Systems Center Energy Conversion Dept. ATTN: CODE 5B331, R. S. Lazar Tech Lib Newport, RI 02840
4	Commander Naval Weapons Center ATTN: Code 388, R. L. Derr C. F. Price T. Boggs Info. Sci. Div. China Lake, CA 93555-6001
2	Superintendent Naval Postgraduate School Department of Mechanical Engineering Monterey, CA 93943-5100
1	Program Manager AFOSR Directorate of Aerospace Sciences ATTN: L. H. Caveny Bolling AFB, DC 20332-0001
6	Commander Naval Ordnance Station ATTN: P. L. Stang J. Birkett L Torreyson T. C. Smith D. Brooks Tech Library Indian Head, MD 20640-5000
1	AFSC/SDOA Andrews AFB, MD 20334
3	AFRPL/DY, Stop 24 ATTN: J. Levine/DYCR R. Corley/DYC D. Williams/DYCC Edwards AFB, CA 93523-5000
1	AFFDL ATTN: TST-Lib Wright-Patterson AFB, OH 45433
1	AFRPL/TSTL (Tech Library) Stop 24 Edwards AFB, CA 93523-5000
1	AFATL/DLYV Eglin AFB, FL 32542-5000
1	AFATL/DLXP Eglin AFB, FL 32542-5000
1	AFATL/DLJE Eglin AFB, FL 32542-5000
1	AFATL/DLODL ATTN: Tech Lib Eglin AFB, FL 32542-5000
1	AFWL/SUL Kirtland AFB, NM 87117

DISTRIBUTION LISTS

No. Of Copies	Organization
1	NASA/Lyndon B. Johnson Space Center ATTN: NHS-22, Library Section Houston, TX 77054
1	AFELM, The Rand Corporation ATTN: Library D (Required or 1700 Main Street Classified Santa Monica CA Only) 90401-3297
1	General Applied Sciences Lab ATTN: J. Erdos Merrick & Stewart Avenues Westbury Long Isld, NY 11590
1	AAI Corporation ATTN: J. Hebert J. Frankle P. O. Box 6767 Baltimore, MD 21204
1	Aerodyne Research, Inc. Bedford Research Park ATTN: V. Yousefian Bedford, MA 01730-1497
1	Aerojet Ordnance Company ATTN: D. Thatcher 2521 Michelle Drive Tustin, CA 92680-7014
1	Aerojet Solid Propulsion Co. ATTN: P. Micheli Sacramento, CA 95813
1	Atlantic Research Corporation ATTN: M. K. King 5390 Cheorokee Avenue Alexandria, VA 22312-2302
1	AVCO Everett Rsch Lab ATTN: D. Stickler 2385 Revere Beach Parkway Everett, MA 02149-5936
2	Calspan Corporation ATTN: C. Morphy P. O. Box 400 Buffalo, NY 14225-0400
10	Central Intelligence Agency Office of Central Reference Dissemination Branch Room GE-47 HQS Washington, DC 20505
1	Foster Miller Associates ATTN: A. Erickson 135 Second Avenue Waltham, MA 02154
1	General Electric Company Armament Systems Dept. ATTN: M. J. Bulman, Room 1311 128 Lakeside Avenue Burlington, VT 05401-4985
1	IITRI ATTN: M. J. Klein 10 W. 35th Street Chicago, IL 60616-3799
1	Hercules Inc. Allegheny Ballistics Laboratory ATTN: R. B. Miller P. O. Box 210 Cumberland, MD 21501-0210
1	Hercules, Inc. Bacchus Works ATTN: K. P. McCarty P. O. Box 98 Magna, UT 84044-0098
1	Hercules, Inc. Radford Army Ammunition Plant ATTN: J. Pierce Radford, VA 24141-0299

DISTRIBUTION LIST

No. Of Copies	Organization
1	Honeywell, Inc. - MN64 2200 Defense Systems Division ATTN: C. Hargreaves 6110 Blue Circle Drive Minnetonka MN 55436
1	Lawrence Livermore National Laboratory ATTN: L-355, A. Buckingham M. Finger P. O. Box 808 Livermore, CA 94550-0622
1	Lawrence Livermore National Laboratory ATTN: L-324 M. Constantino P. O. Box 808 Livermore, CA 94550-0622
1	Olin Corporation Badger Army Ammunition Plant ATTN: R. J. Thiede Baraboo, WI 53913
1	Olin Corporation Smokeless Powder Operations ATTN: D. C. Mann P.O. Box 222 St. Marks, FL 32355-0222
1	Paul Gough Associates, Inc. ATTN: P. S. Gough P. O. Box 1614, 1048 South St. Portsmouth, NH 03801-1614
1	Physics International Company ATTN: Library H. Wayne Wampler 2700 Merced Street San Leandro, CA 94577-5602
1	Princeton Combustion Research Lab., Inc. ATTN: M. Summerfield 475 US Highway One Monmouth Junction, NJ 08852-9650
2	Rockwell International Rocketdyne Division ATTN: BA08 J. E. Flanagan J. Gray 6633 Canoga Avenue Canoga Park, CA 91303-2703
1	Science Applications, Inc. ATTN: R. B. Edelman 23146 Cumorah Crest Drive Woodland Hills, CA 91364-3710
3	Thiokol Corporation Huntsville Division ATTN: D. Flanigan R. Glick Tech Library Huntsville, AL 35807
1	Scientific Research Assoc., Inc. ATTN: H. McDonald P.O. Box 498 Glastonbury, CT 06033-0498
1	Thiokol Corporation Wasatch Division ATTN: J. A. Peterson P. O. Box 524 Brigham City, UT 84302-0524
2	Thiokol Corporation Elkton Division ATTN: R. Biddle Tech Lib. P. O. Box 241 Elkton, MD 21921-0241

DISTRIBUTION LIST

No. Of Copies	Organization
2	United Technologies Chemical Systems Division ATTN: R. Brown Tech Library P. O. Box 358 Sunnyvale, CA 94086-9998
1	Veritay Technology, Inc. ATTN: E. Fisher 4845 Millersport Hwy. P. O. Box 305 East Amherst, NY 14051-0305
1	Universal Propulsion Company ATTN: H. J. McSpadden Black Canyon Stage 1 Box 1140 Phoenix, AZ 85029
1	Battelle Memorial Institute ATTN: Tech Library 505 King Avenue Columbus, OH 43201-2693
1	Brigham Young University Dept. of Chemical Engineering ATTN: M. Beckstead Provo, UT 84601
1	California Institute of Tech 204 Karman Lab Main Stop 301-46 ATTN: F. E. C. Culick 1201 E. California Street Pasadena, CA 91109
1	California Institute of Tech Jet Propulsion Laboratory ATTN: L. D. Strand 4800 Oak Grove Drive Pasadena, CA 91109-8099
1	University of Illinois Dept of Mech/Indust Engr ATTN: H. Krier 144 MEB; 1206 N. Green St. Urbana, IL 61801-2978
1	University of Massachusetts Dept. of Mechanical Engineering ATTN: K. Jakus Amherst, MA 01002-0014
1	University of Minnesota Dept. of Mechanical Engineering ATTN: E. Fletcher Minneapolis, MN 55414-3368
1	Case Western Reserve University Division of Aerospace Sciences ATTN: J. Tien Cleveland, OH 44135
3	Georgia Institute of Tech School of Aerospace Eng. ATTN: B. T. Zinn E. Price W. C. Strahle Atlanta, GA 30332
1	Institute of Gas Technology ATTN: D. Gidaspow 3424 S. State Street Chicago, IL 60616-3896
1	Johns Hopkins University Applied Physics Laboratory Chemical Propulsion Information Agency ATTN: T. Christian Johns Hopkins Road Laurel, MD 20707-0690
1	Massachusetts Institute of Technology Dept of Mechanical Engineering ATTN: T. Toong 77 Massachetts Avenue Cambridge, MA 02139-4307

DISTRIBUTION LIST

No. Of Copies	Organization
1	G. M. Faeth Pennsylvania State University Applied Research Laboratory University Park, PA 16802-7501
1	Pennsylvania State University Dept. Of Mech. Engineering ATTN: K. Kuo University Park, PA 16802-7501
1	Purdue University School of Mechanical Engineering ATTN: J. R. Osborn TSPC Chaffee Hall West Lafayette, IN 47907-1199
1	SRI International Propulsion Sciences Division ATTN: Tech Library 333 Ravenswood Avenue Menlo Park, CA 94025-3493
1	Rensselaer Polytechnic Inst. Department of Mathematics Troy, NY 12181
2	Director Los Alamos Scientific Lab ATTN: T3, D. Butler M. Division, B. Craig P. O. Box 1663 Los Alamos, NM 87544
1	Stevens Institute of Technology Davidson Laboratory ATTN: R. McAlevy, III Castle Point Station Hoboken, NJ 07030-5907
1	Rutgers University Dept. of Mechanical and Aerospace Engineering ATTN: S. Temkin University Heights Campus New Brunswick, NJ 08903
1	University of Southern California Mechanical Engineering Dept. ATTN: OHE200, M. Gerstein Los Angeles, CA 90089-5199
2	University of Utah Dept. of Chemical Engineering ATTN: A. Baer G. Flandro Salt Lake City, UT 84112-1194
1	Washington State University Dept. of Mechanical Engineering ATTN: C. T. Crowe Pullman, WA 99163-5201

Aberdeen Proving Ground

Dir, USAMSAA
ATTN: AMXSY-D
AMXSY-MP, H. Cohen
Cdr, USATECOM
ATTN: AMSTE-TO-F
AMSTE-CM-F, L. Nealley
Cdr, CSTA
ATTN: STECS-AS-H, R. Hendricksen
Cdr, CRDC, AMCCOM
ATTN: SMCCR-RSP-A
SMCCR-MU
SMCCR-SPS-IL

USER EVALUATION SHEET/CHANGE OF ADDRESS

This Laboratory undertakes a continuing effort to improve the quality of the reports it publishes. Your comments/answers to the items/questions below will aid us in our efforts.

1. BRL Report Number _____ Date of Report _____

2. Date Report Received _____

3. Does this report satisfy a need? (Comment on purpose, related project, or other area of interest for which the report will be used.) _____

_____

_____

4. How specifically, is the report being used? (Information source, design data, procedure, source of ideas, etc.) _____

_____

_____

5. Has the information in this report led to any quantitative savings as far as man-hours or dollars saved, operating costs avoided or efficiencies achieved, etc? If so, please elaborate. _____

_____

_____

6. General Comments. What do you think should be changed to improve future reports? (Indicate changes to *organization, technical content, format, etc.*)

_____

_____

_____

CURRENT ADDRESS

_____
Name

_____
Organization

_____
Address

_____
City, State, Zip

7. If indicating a Change of Address or Address Correction, please provide the New or Correct Address in Block 6 above and the Old or Incorrect address below.

OLD ADDRESS

_____
Name

_____
Organization

_____
Address

_____
City, State, Zip

(Remove this sheet along the perforation, fold as indicated, staple or tape closed, and mail.)

END

DTIC

7-86